April 2013

Synthesis, Spectroscopic Properties, and Photophysical Properties of (2E,5E)-2-benzylidene-5-(p-dimethylaminocinnamylidene)-cyclopentanone (bdmac)

Cara Lynn DiIorio
Worcester Polytechnic Institute

Project Number: MQP-REC-0045

Synthesis, Spectroscopic Properties, and Photophysical Properties of (2E,5E)-2-benzylidene-5-(p-dimethylaminocinnamylidene)-cyclopentanone (bdmac)

A Major Qualifying Project Report

Submitted to the Faculty

Of the

WORCESTER POLYTECHNIC INSTITUTE

In partial fulfillment of the requirements for the

Degree of Bachelor of Science

By

Cara L. DiIorio

on

April 25, 2013

Approved by:

_____

Professor Robert E. Connors, Ph.D.

Project Advisor

Table of Contents

List of Figures

List of Tables

Abstract

This project extends previous studies of the spectroscopic and photophysical properties of 2,5-diarylidene cyclopentanones. The focus of this research is (2E,5E)-2-benzylidene-5-(p-dimethylaminocinnamylidene)-cyclopentanone (bdmac), a new compound that was synthesized in two steps. First, (E)-2-benzylidene-cyclopentanone (1pdbun) was synthesized using DIMCARB catalyst; a base-catalyzed crossed aldol condensation between 1pdbun and (E)-p-dimethylaminocinnamaldehyde was the second step.

Investigation of bdmac's spectral properties involved obtaining its absorbance and fluorescence spectra in a variety of solvents. Bdmac was found to exhibit solvatochromism; bathochromic shifts were observed in spectral maxima with increasing solvent polarity. Bdmac was not found to exhibit excited state proton transfer in glacial acetic acid. More data must be gathered to determine whether bdmac exhibits phosphorescence in frozen methylcyclohexane.

The photophysical properties of bdmac, including fluorescence quantum yields and lifetimes, also vary with solvent polarity. First-order radiative and non-radiative decay constants were calculated from quantum yield and lifetime data. Flash photolysis and photochemistry studies were conducted as well. Finally, geometry optimization and spectral calculations performed at the B3LYP/6-311+G(d,p) level of theory revealed the internal charge transfer nature of bdmac.

Results from the above experiments were compared to data obtained previously for (2E,5E)-2-(p-dimethylaminobenzylidene)-5-(p-dimethylaminocinnamylidene)-cyclopentanone (Ashrbor), a related compound.

Acknowledgements

I would like to thank Professor Robert Connors for the use of his lab and for his valuable and enthusiastic guidance throughout the course of this project. I would also like to thank Laura Murray for enduring with me those long afternoons spent in the lab collecting fractions from columns and dealing with disobedient computers and lab equipment. I would like to thank Paula Moravek, Mary Ballard, and Rebecca Evanoff for helping me with various tasks throughout the year. For his endless patience, advice, and time, I would like to thank Chris Zoto. Finally, my thanks to Professor Christopher Lambert for his generous donation of time and for the use of his laser flash photolysis (LFP) system.

Introduction

The focus of this project is the compound (2E,5E)-2-benzylidene-5-(p-dimethylaminocinnamylidene)-cyclopentanone (bdmac), a member of the family of 2,5-diarylidene cyclopentanones. *Figure 1* gives the general structure of these highly conjugated compounds. Conjugated compounds contain a system of alternating single and double bonds whose overlapping *p* orbitals allow for electron delocalization within the molecule.

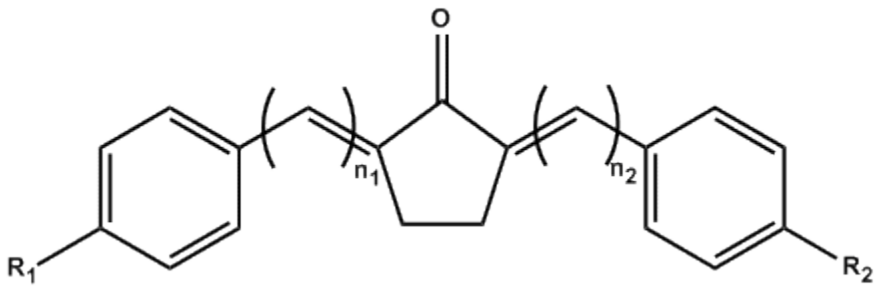

Figure 1: Structure of 2,5-diarylidene cyclopentanones

The 2,5-diarylidene cyclopentanones can be either symmetrically or asymmetrically substituted. Symmetric compounds, in which $R_1 = R_2$ and $n_1 = n_2$, have C_{2v} symmetry, while asymmetric compounds like bdmac have only C_1 symmetry. For these compounds, R_1 and R_2 differ, or n_1 and n_2 differ. All four variables may also be unique, as can be noted from the structure of bdmac presented in *Figure 2*.

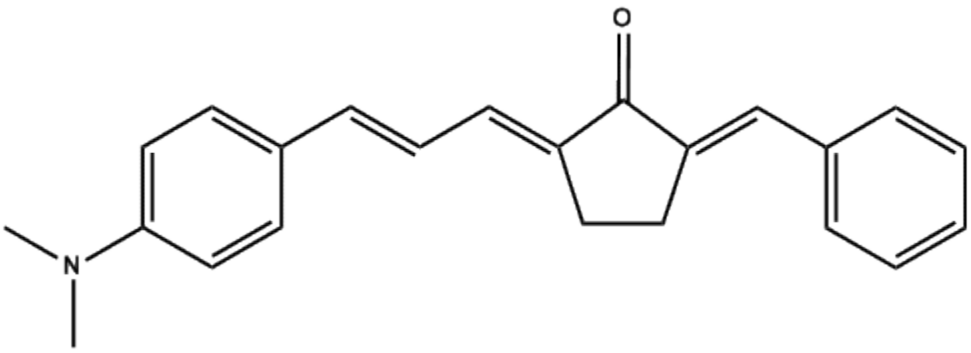

Figure 2: Structure of bdmac

Recently, several applications of the 2,5-diarylidene cyclopentanones have been discovered. They can be used as fluoroionophores, fluorescent solvent polarity probes, and nonlinear optical materials [4]. The compounds exhibit two-photon absorbance (TPA) [14]. They can also be used as photosensitizers, which have applications in cancer treatment. In photodynamic therapy, tumors are targeted with photosensitizers and then irradiated with an intense pulse of light. This causes the photosensitizer to generate singlet oxygen from ambient triplet (ground state) oxygen, causing cell destruction [15]. Use in fluorescence multilayer discs (FMDs) is another application of the compounds. These discs utilize fluorescent compounds to store data, and they can store much more information than traditional compact discs of the same size [10].

The various applications of the 2,5-diarylidene cyclopentanones are related to their interesting spectroscopic and photophysical properties. For instance, it has been shown that these compounds exhibit solvatochromism, a phenomenon in which solutions of a compound vary in color with varying solvent polarity. In other words, the absorbance and fluorescence maxima of these compounds depend on the polarity of the solvent in which they are dissolved. In the case of the 2,5-diarylidene cyclopentanones, there is an observed bathochromic (red) shift in spectral maxima with increasing solvent polarity. As the solvent becomes more polar, the maximum absorbance and fluorescence occur at increasingly longer wavelengths and correspondingly lower energies [3, 4, 6, 9, 10, 11, 14, 15]. A hypsochromic (blue) shift is the opposite situation; absorbance and fluorescence maxima occur at increasingly shorter, higher-energy wavelengths with increasing solvent polarity [1, 6].

Zoto and Connors recently reported that an internal charge transfer occurs in the transition from S_0 (the ground state) to S_1 (the first excited singlet state) in (2E,5E)-2-(p-dimethylaminobenzylidene)-5-(p-cyanobenzylidene)-cyclopentanone (I), an asymmetrically substituted 2,5-diarylidene cyclopentanone [14]. Electron density shifts from the electron donor end of the molecule in the HOMO to the electron acceptor end in the LUMO upon excitation to

S_1, supporting evidence that I interacts more strongly with polar solvents than with nonpolar solvents [14]. This may account for the observed bathochromic shift in the absorbance and fluorescence maxima of the 2,5-diarylidene cyclopentanones with increasing solvent polarity. For I, the $S_0 \rightarrow S_1$ transition is (π, π^*) and strongly observed, while the $S_0 \rightarrow S_2$ transition is (n, π^*) and weakly observed [14].

Connors and Ucak-Astarlioglu have done extensive studies on a set of three symmetric 2,5-diarylidene cyclopentanones [4, 5]. First, they reported on the photophysical and spectroscopic properties of these compounds in a variety of organic solvents [4]. Their subsequent work focused on determining whether excited state proton transfer takes place in these compounds when dissolved in acidic media at room temperature. Through a computational and spectroscopic experimental approach, they found that two of the three compounds exhibit S_1 excited state proton transfer in diluted sulfuric acid and glacial acetic acid [5].

In diluted sulfuric acid, both protonated and unprotonated species exist in the ground state, as indicated by the presence of two absorbance bands. However, only the protonated form exists in the excited state because there is only one emission band. This indicates that the unprotonated species in the ground state must undergo proton transfer in the excited state prior to emission. In acetic acid, neither of the two compounds is protonated in the ground state, as evidenced by the presence of only one absorbance band. The fluorescence spectra of the compounds shows two emission bands, indicating the presence of both protonated and unprotonated species in the excited state. Therefore, a proportion of the unprotonated species undergo excited state proton transfer before emission [5].

One reason for the occurrence of excited state proton transfer is that the $S_0 \rightarrow S_1$ transition is (π, π^*) [5]. When the molecules are excited to the first excited singlet state, there is a transfer of electron density to the carbonyl oxygen, much like Zoto and Connors reported for compound I [5, 14]. This makes the molecule a stronger base in the excited state and therefore

more likely to accept a proton from an acid. On the other hand, if the $S_0 \rightarrow S_1$ transition is (n, π^*), the electron density on the carbonyl oxygen decreases, making the compound a weaker base in the excited state. As a result, it likely will not exhibit excited state proton transfer [5].

In 2012, Zoto described a competition between excited state photooxidation and photoisomerization of (2E,5E)-2,5-bis-(p-dimethylaminobenzylidene)-cyclopentanone (bis-dmab). Intersystem crossing occurs after bis-dmab is excited to the first excited singlet state. If triplet oxygen is present, the two species react to produce ground state bis-dmab and excited state singlet oxygen, causing a further reaction in which bis-dmab is photooxidized to p-dimethylaminobenzaldehyde and a cyclopentadione product. In the absence of oxygen, (E,E) → (E,Z) photoisomerization follows intersystem crossing [15].

Absorption, radiative transitions, and non-radiative transitions can be shown schematically on a Jablonski diagram, an example of which is shown in *Figure 3*. Radiative transitions involve the emission of energy as a photon and are represented by straight, downward-pointing arrows. Non-radiative transitions are represented by wavy arrows and involve the emission of energy as heat. Horizontal lines denote energy levels and multiplicities; S is a singlet state, and T is a triplet state. Straight vertical arrows pointing upward represent the absorption of energy by a molecule in the form of photons. Absorption can only occur between states of the same multiplicity and must always be accompanied by an eventual relaxation to the ground state [1, 12].

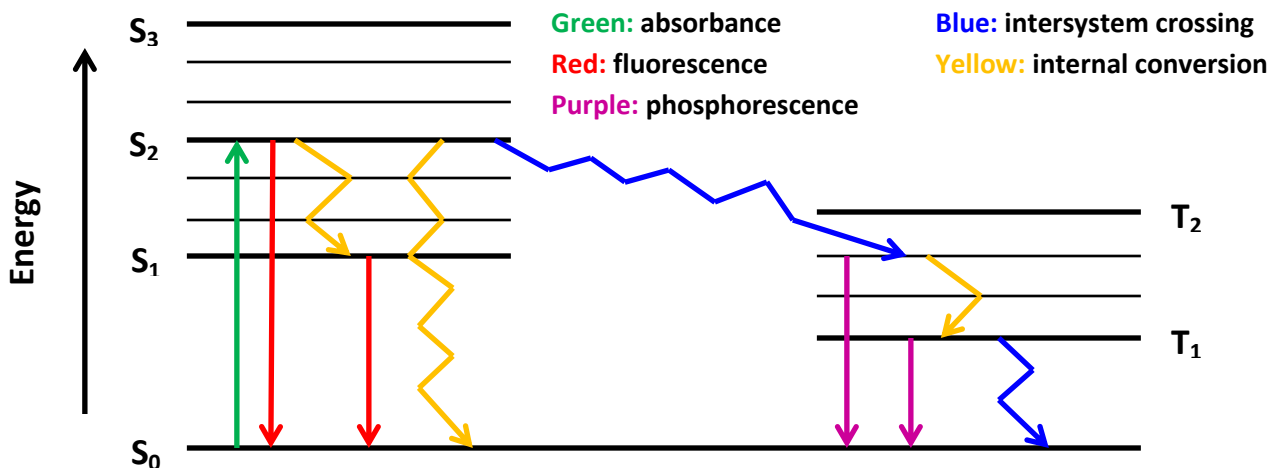

Figure 3: Sample Jablonski diagram

This return to the ground state can be accomplished in numerous ways. The absorbed photons can undergo fluorescence, which is the radiative transition from an excited singlet state to the ground state. This process is spin-allowed and short-lived. Molecules may also undergo internal conversion before fluorescing back to the ground state. Internal conversion is a non-radiative transition between energy levels of the same multiplicity. Internal conversion to the ground state is possible as well [1, 12].

Intersystem crossing, or the non-radiative transition from an excited singlet state to an excited triplet state, can also occur. This process may be followed by phosphorescence, the radiative transition from a higher-energy triplet state to the ground state. Phosphorescence is spin-forbidden and long-lived. The proportion of photons that undergo phosphorescence is a result of competition between fluorescence, internal conversion, and intersystem crossing for a particular compound [1, 2, 12]. Molecules can undergo internal conversion before undergoing phosphorescence as well. The final option is to undergo internal conversion to T_1 and then undergo intersystem crossing in order to relax back to the ground state [1, 12].

Triplet states of compounds can be analyzed using laser flash photolysis, a technique in which a change in absorbance is measured in response to an intense pulse of light. In this method, a laser excites molecules into the S_1 excited state. Then intersystem crossing occurs,

causing some photons to enter the T_1 excited state. The photons are then excited again to a higher-energy triplet state (T_n). Utilization of this technique makes it possible to measure the lifetimes of triplet states by studying the rate of decay for $T_1 \rightarrow S_0$ [2].

The fluorescence quantum yield of a compound is the proportion of total absorbed photons that fluoresce from a sample. Other photons may generate internal conversion, intersystem crossing, and/or phosphorescence. Similarly, the phosphorescence quantum yield is the percentage of total absorbed photons that phosphoresce from a sample. In contrast, the quantum efficiency of phosphorescence refers to the proportion of photons that undergo phosphorescence after undergoing intersystem crossing to some excited triplet state. Fluorescence lifetimes are usually on the order of nanoseconds, while lifetimes of triplet states are usually in the microsecond range. The radiative and non-radiative decay rates of photophysical processes can be calculated from quantum yields and lifetimes [1, 14].

The objectives of this project were to synthesize bdmac, examine the compound's spectroscopic and photophysical properties, and analyze any observed trends. To this end, the absorbance and fluorescence spectra of bdmac were obtained in various solvents differing in polarity, as well as in glacial acetic acid and methylcyclohexane. Fluorescence quantum yields and lifetimes were also measured. Flash photolysis studies were conducted, as were photochemistry experiments. In addition, theoretical quantum chemical calculations were performed, including geometry optimization and TD-DFT spectral calculations. Results were then compared to those obtained for another 2,5-diarylidene cyclopentanone.

Experimental

I. Synthesis of bdmac

a. DIMCARB-Catalyzed Synthesis of (E)-2-benzylidene-cyclopentanone (1pdbun)

The reaction scheme for the synthesis of 1pdbun is shown schematically in *Figure 4*. Dichloromethane (5.8 mL) was added to a round bottom flask, followed by benzaldehyde (5.0 mmol, 0.51 mL), DIMCARB (3.3 mL), and cyclopentanone (5.0 mmol, 0.44 mL). The reaction mixture was kept at room temperature with continuous stirring for 24 hours, at which point the solvent was removed *in vacuo*. Sulfuric acid (0.5 M, 10 mL) was added in several portions in order to neutralize any remaining DIMCARB. The mixture was then separated via a 3 x 25 mL ethyl acetate extraction. The organic layer was dried over sodium sulfate, and the ethyl acetate was removed *in vacuo* [8, 15].

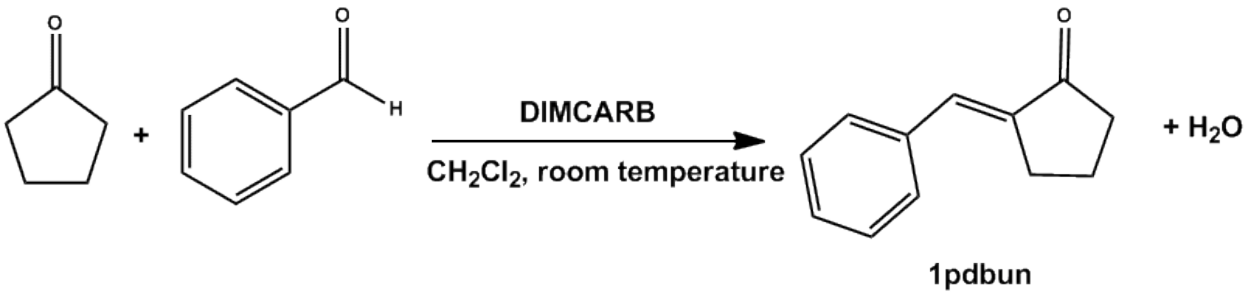

Figure 4: Reaction scheme for the synthesis of 1pdbun

The presence of 1pdbun in the crude product was confirmed by ^{1}H NMR. Purification of the crude product consisted of silica gel column chromatography using a hexanes/ethyl acetate gradient approach. Polarity of the liquid phase was gradually increased by increasing the ethyl acetate concentration. A total of 0.35 g of 1pdbun was recovered after purification (41% recovery). The identity of the product was confirmed by ^{1}H and ^{13}C NMR spectroscopy. The resulting spectra and spectral data, shown in *Figures 5 – 9* and *Table 1*, respectively, agree with previously published data on 1pdbun [15]. An extra hydrogen atom is observed in the ^{1}H NMR

spectrum in the multiplet between δ7.20 and δ7.31; this can be attributed to the residual $CDCl_3$ solvent peak at δ7.26 [7].

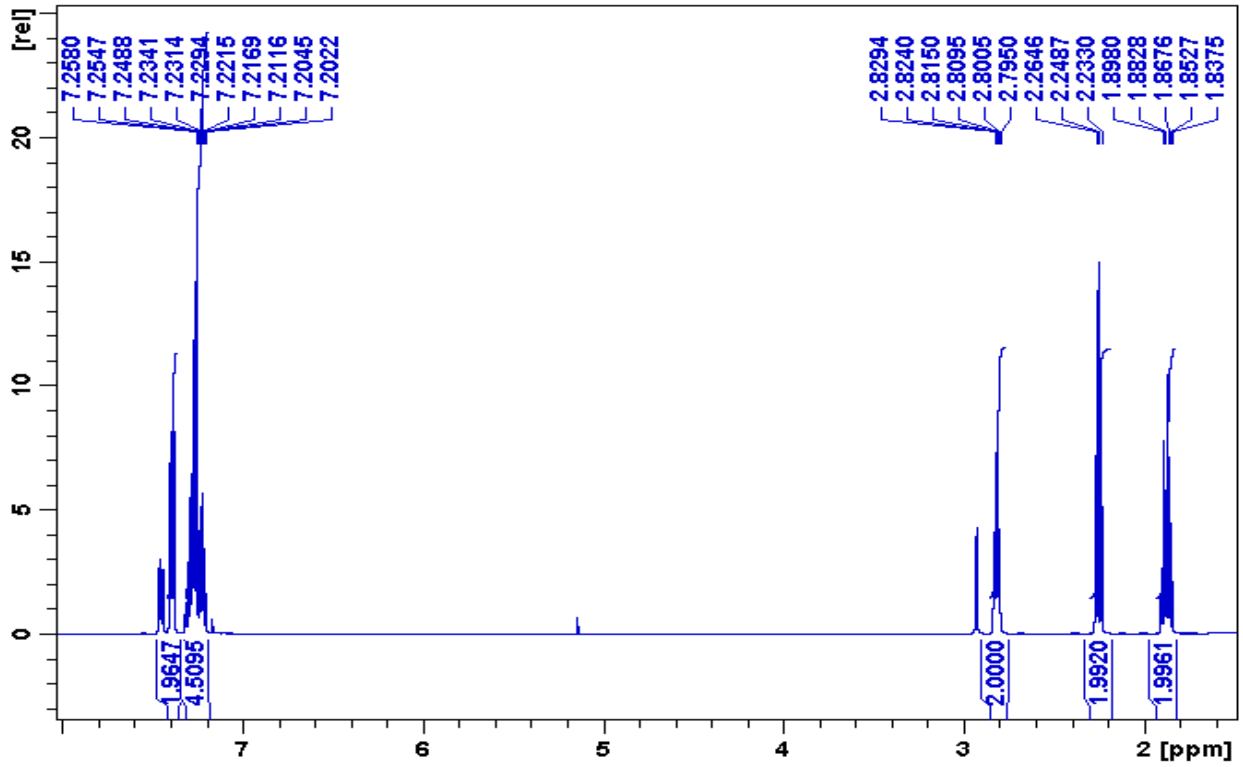

Figure 5: ^{1}H NMR spectrum of 1pdbun, δ1.5 – 8.0 ppm

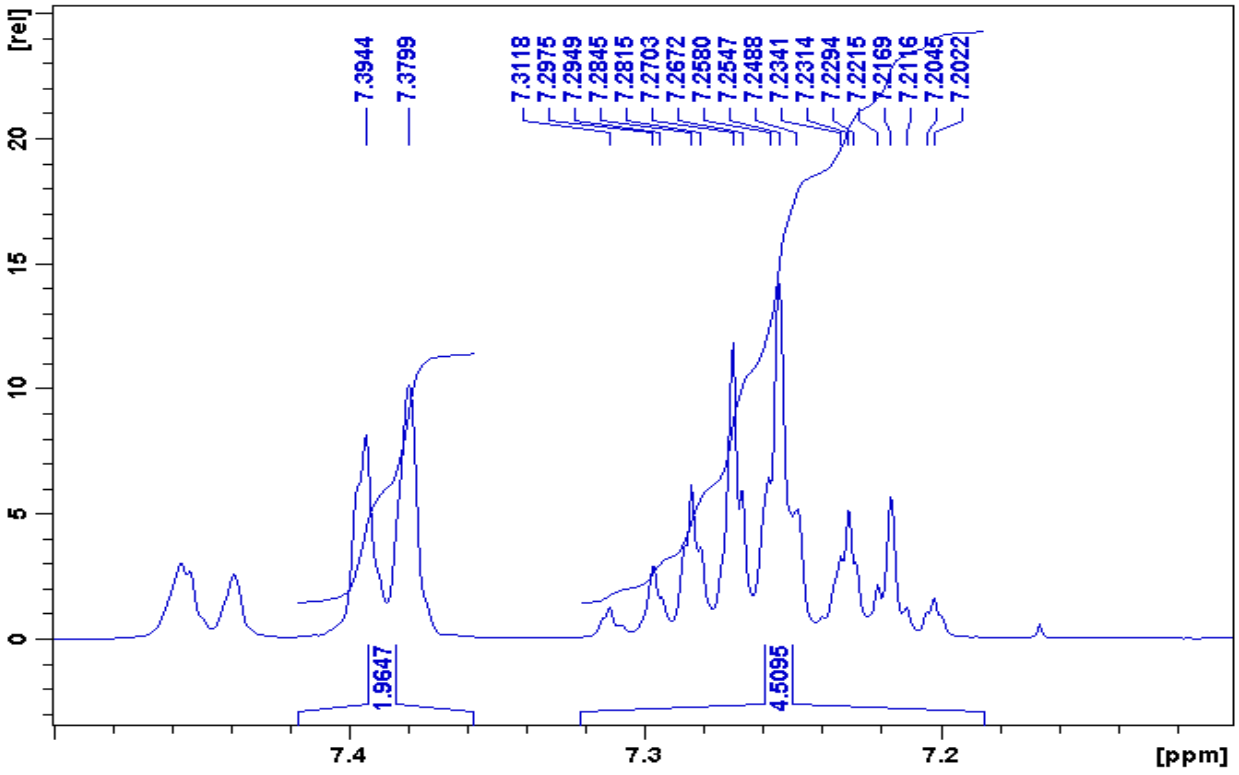

Figure 6: ^{1}H NMR spectrum of 1pdbun, δ7.1 – 7.5 ppm

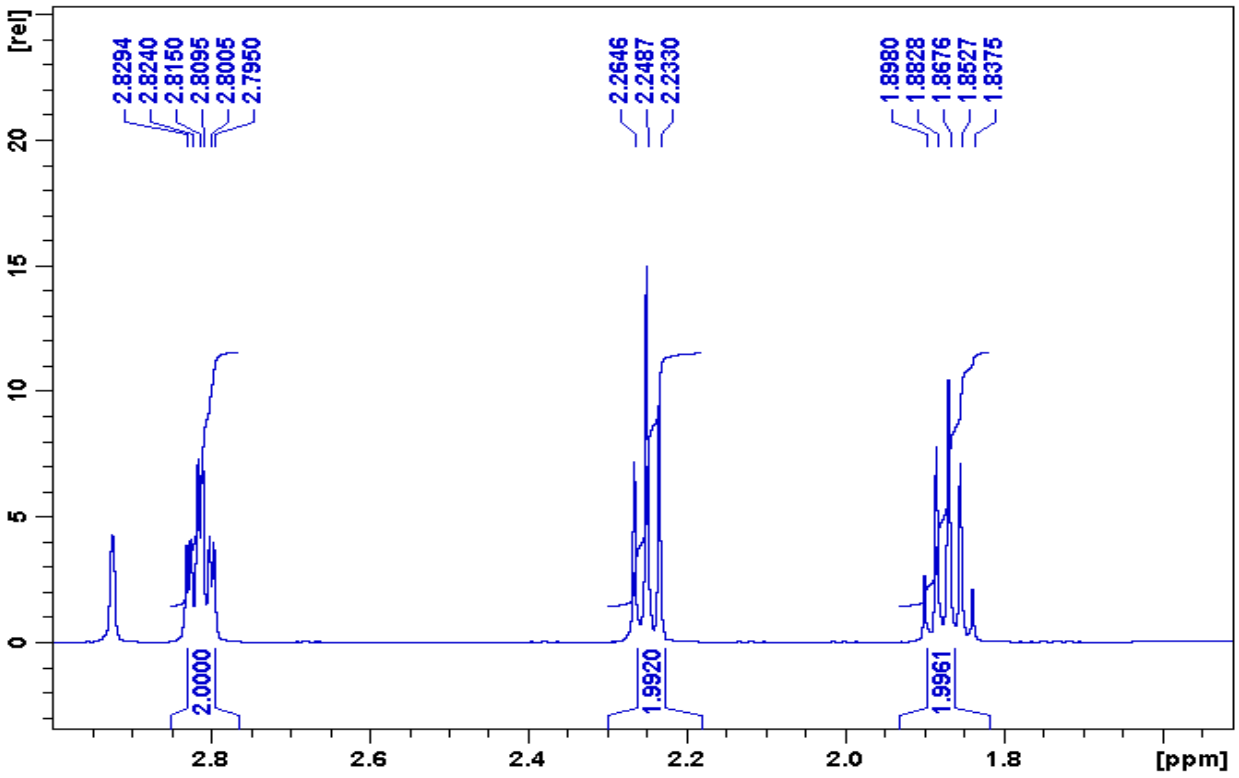

Figure 7: ^{1}H NMR spectrum of 1pdbun, δ1.5 – 3.0 ppm

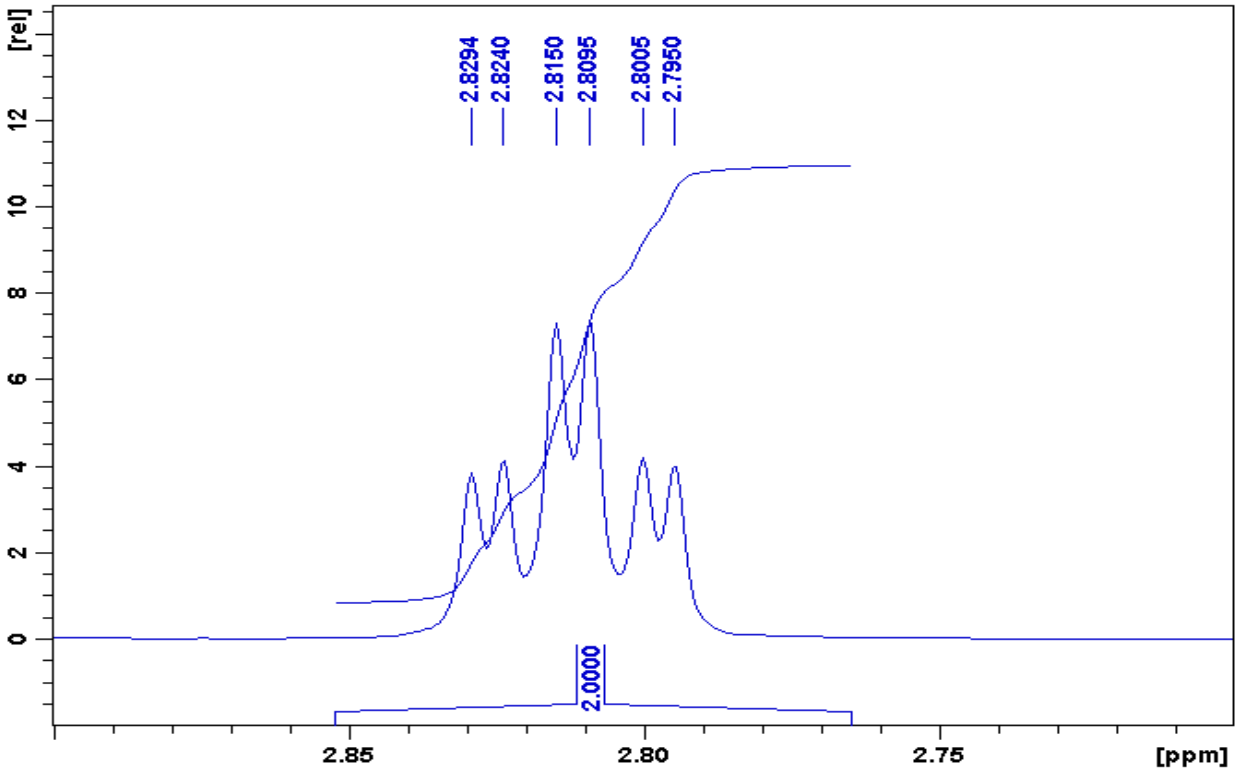

Figure 8: ^{1}H NMR spectrum of 1pdbun, δ2.7 – 2.9 ppm

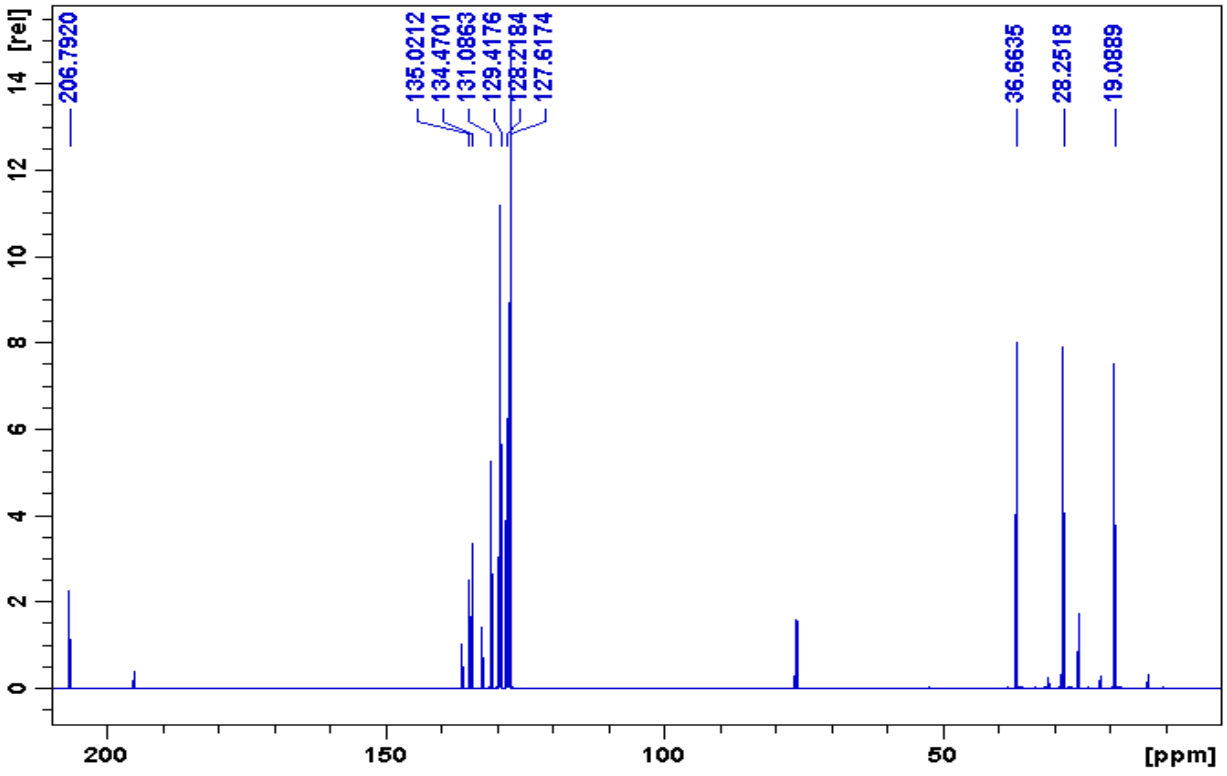

Figure 9: ^{13}C NMR spectrum of 1pdbun, δ0 – 210 ppm

b. Base-catalyzed synthesis of bdmac

Bdmac was synthesized via an intermolecular base-catalyzed crossed aldol condensation, as shown in *Figure 10*. 1pdbun (1.16 mmol, 0.2 g) was placed in an Erlenmeyer flask along with ethanol (50 mL). The solution was allowed to stir. (E)-p-dimethylaminocinnamaldehyde (1.16 mmol, 0.2 g) was placed in a second Erlenmeyer flask and dissolved in ethanol (75 mL) via continuous stirring. Once complete dissolution of 1pdbun had occurred, NaOH (2.5% w/v in DI H_2O, 2 mL) was added to the ketone solution. The resulting mixture was allowed to stir for 30 minutes. The aldehyde solution was then added by pipet to the 1pdbun mixture. A color change from yellow to deep red was observed upon addition of the aldehyde. The reaction mixture was allowed to proceed overnight with constant stirring at room temperature.

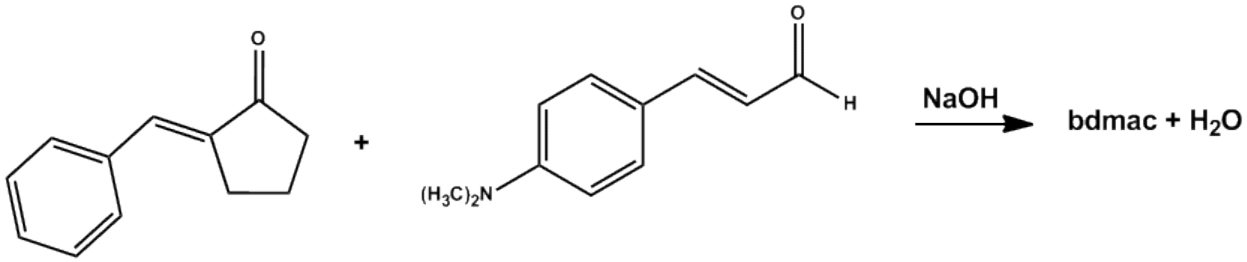

Figure 10: Reaction scheme for the synthesis of bdmac

After 24 hours, a reddish-brown precipitate was observed. The precipitate was collected by vacuum filtration, washed with cold ethanol, and dried for 1 hour. Presence of bdmac in the crude precipitate was confirmed by ^{1}H NMR and TLC, and it was purified via silica gel column chromatography. The solvent system used was a 1:4 mixture of ethyl acetate and hexanes.

Purity of the final product was confirmed by TLC, which showed one spot upon development. A total of 0.2945 g of the pure product was recovered (78% recovery). Melting point measurements were attempted three times, but bdmac decomposed at 163°C. Identity of the product was confirmed by ^{1}H and ^{13}C NMR spectroscopy. The spectra are shown in *Figures 13 – 20*, and spectral data is shown in *Table 1*. The IR spectrum and spectral data of bdmac are shown in *Figure 21* and *Table 2*, respectively.

Figure 11 below gives the structure of bdmac with alphabetical labels to indicate which hydrogen atoms in the molecule are in the same chemical environment. Each group corresponds to one signal in the ^{1}H NMR spectrum. Similarly, *Figure 12* gives bdmac's structure with each unique carbon group labeled numerically. Since bdmac is an asymmetric molecule, the left and right sides are not chemically equivalent.

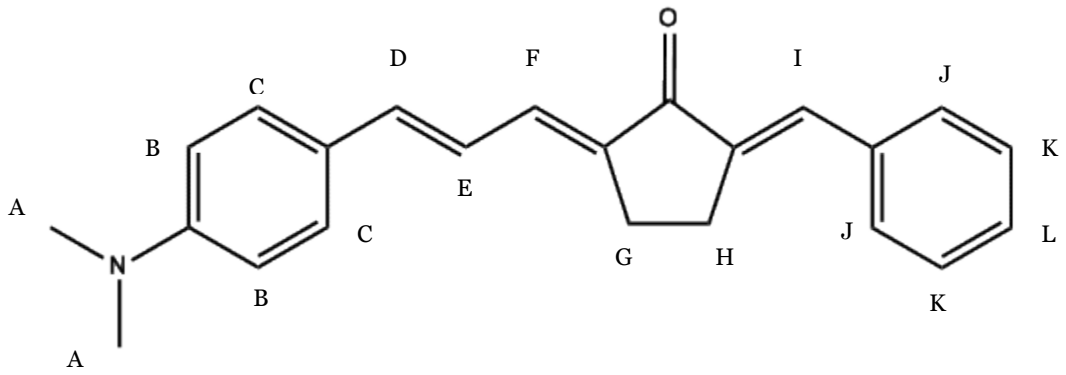

Figure 11: Structure of bdmac with labeled hydrogen groups

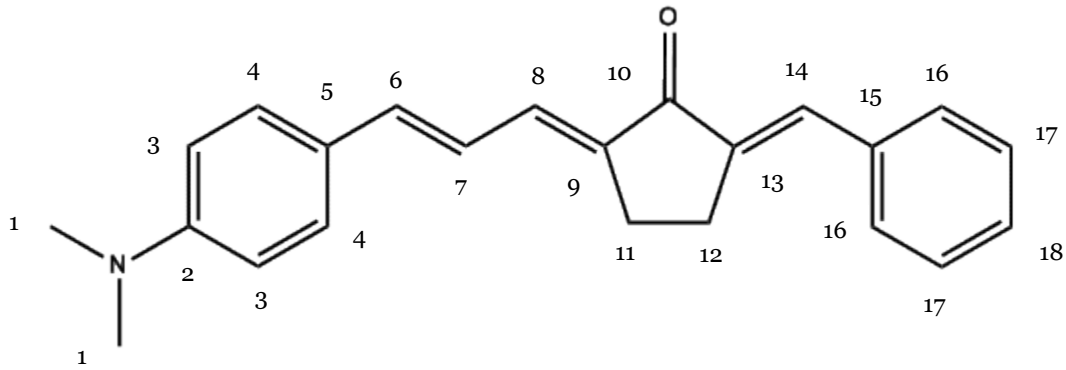

Figure 12: Structure of bdmac with labeled carbon groups

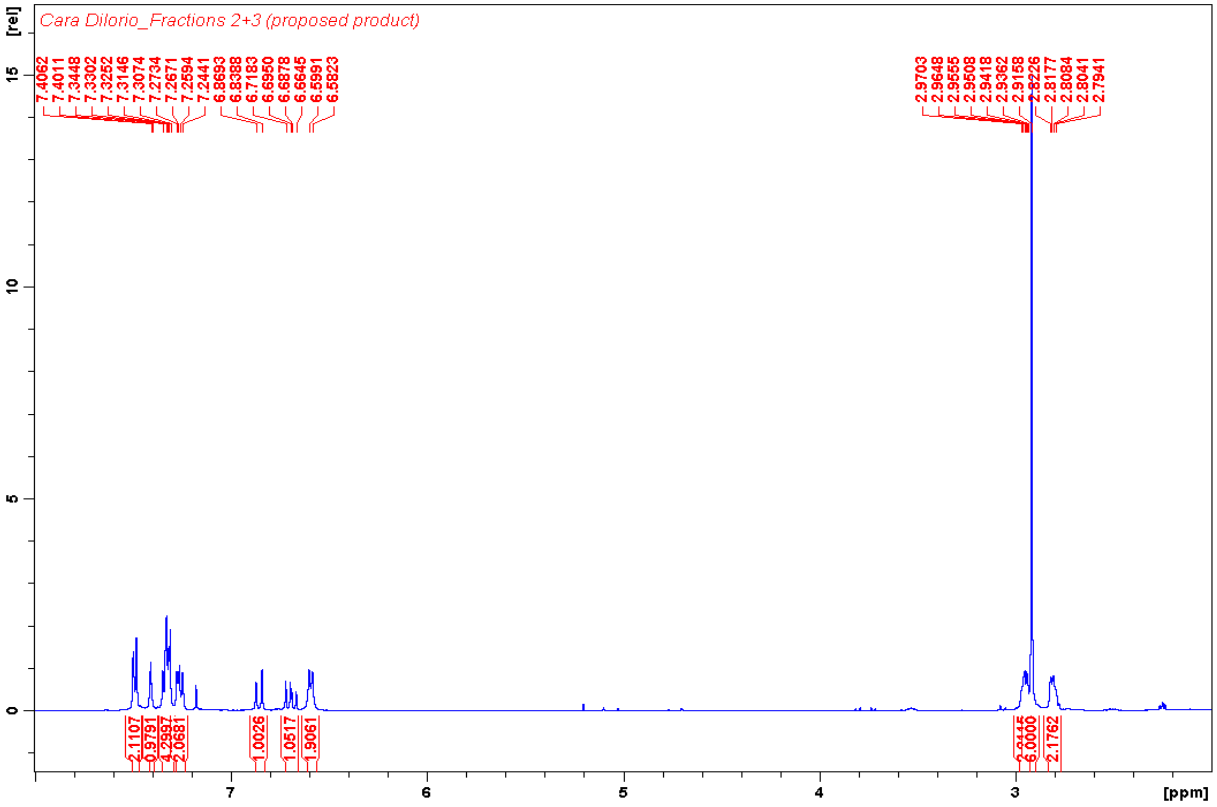

Figure 13: ^{1}H NMR spectrum of bdmac, δ2.0 – 8.0 ppm

Figure 14 shows the aliphatic region of the ^{1}H NMR spectrum of bdmac. The singlet at δ2.91 integrates to six hydrogens and therefore must correspond to group A (see *Figure 11*). Each of the multiplets integrates to two hydrogens. These signals must correspond to the two methylene groups on the cyclopentanone ring (groups G and H), which are the only other aliphatic hydrogen groups in the molecule.

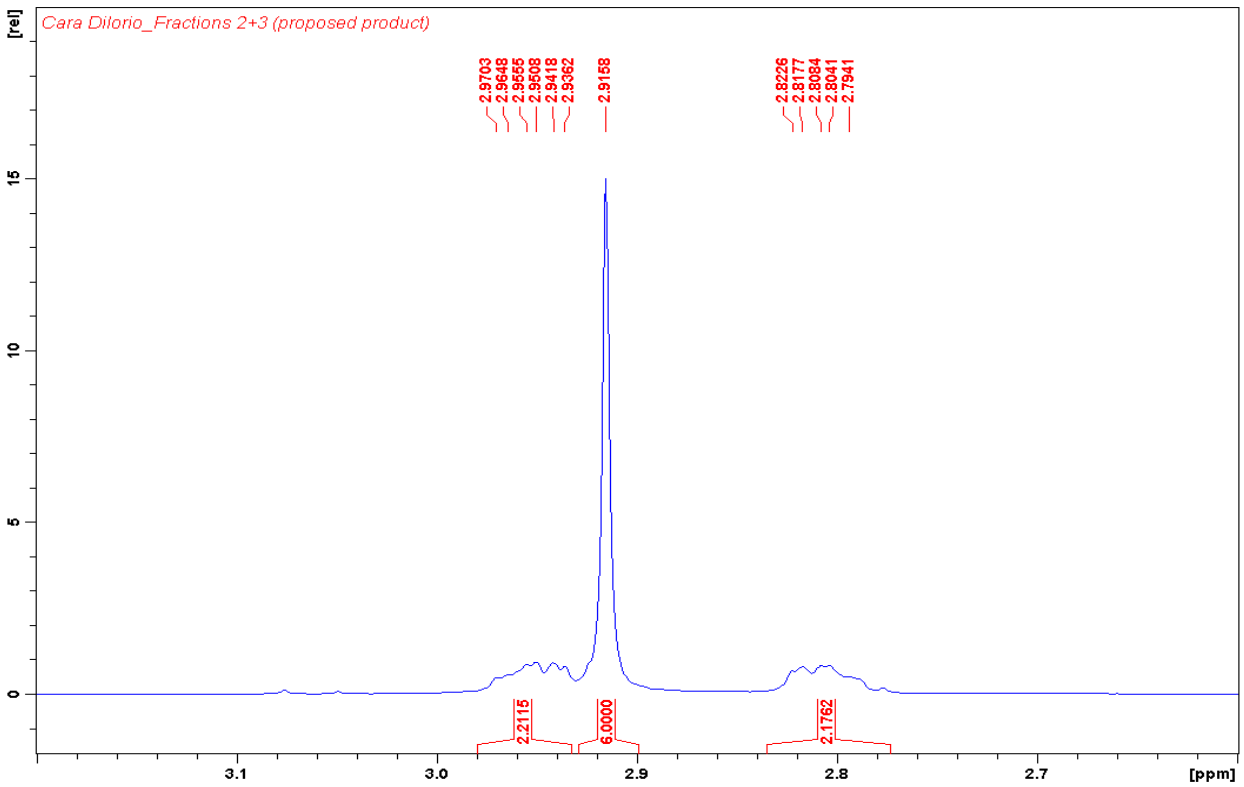

Figure 14: ^{1}H NMR spectrum of bdmac, δ2.6 – 3.2 ppm

Figure 15 shows the aromatic region of bdmac's ^{1}H NMR spectrum. The doublet at δ7.49 integrates to two hydrogens, so it could correspond to groups B or C (see *Figure 11*). The triplet at δ7.40 integrates to one hydrogen and corresponds to group E. The four-hydrogen multiplet at δ7.34 – 7.30 seems to be an overlap of the two signals from groups J and K. The two-hydrogen multiplet at δ7.27 – 7.24 is likely to be the overlapping signals from groups F and I. The signal at δ6.86 is a doublet integrating to one hydrogen and therefore most likely corresponds to group D. The multiplet at δ6.71 – 6.66 integrates to one hydrogen and corresponds to group L. Finally, the two-hydrogen doublet at δ6.59 corresponds to either group B or C.

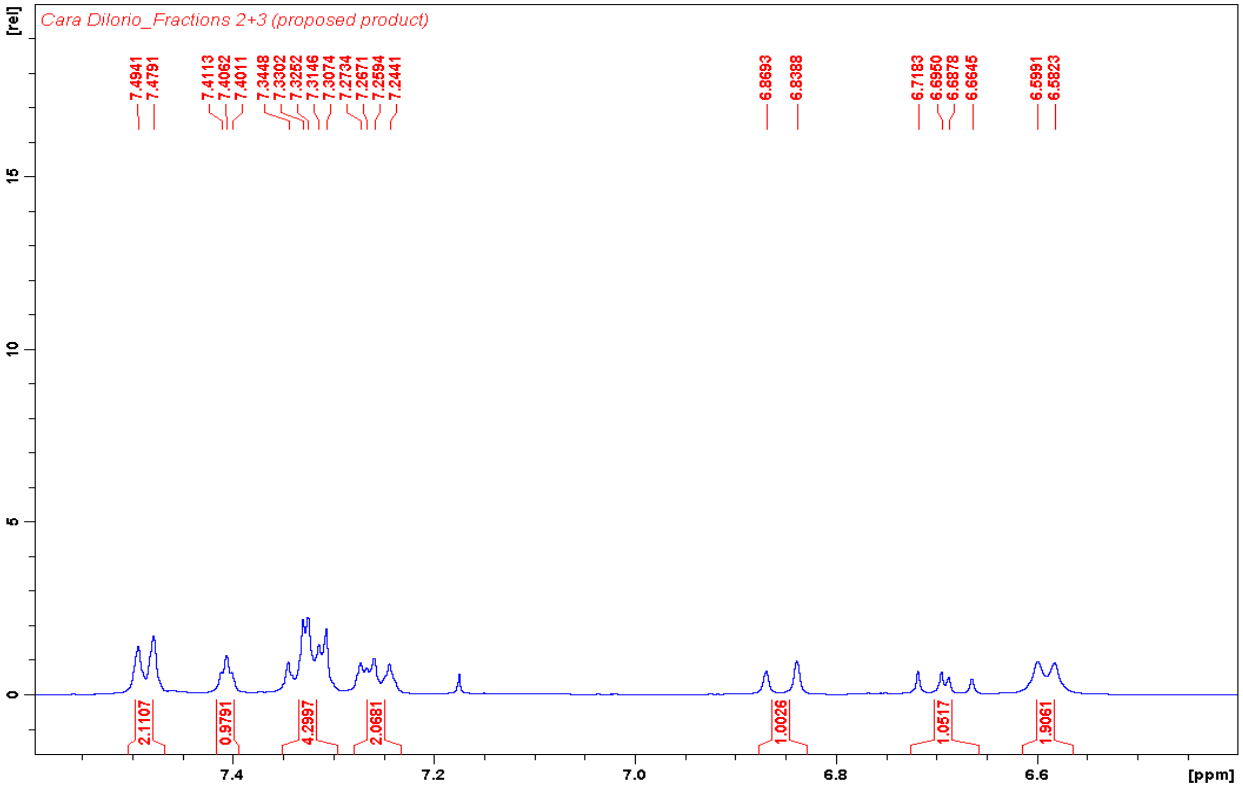

Figure 15: ^{1}H NMR spectrum of bdmac, δ6.4 – 7.6 ppm

Figures 16 – 20 show the various ^{13}C NMR spectra collected for bdmac. The complete proton decoupling spectrum (*Figure 16)* shows signals for all carbon groups in the molecule. Of note are the signals at δ23.3, 25.1, 39.2, and 194.3, which correspond to groups 11, 12, 1, and 10, respectively (see *Figure 12*). There are nine signals observed in the DEPT-90 spectrum shown in *Figure 17*, which is consistent with the number of unique CH groups in bdmac. The DEPT-135 spectrum, shown in *Figures 18 – 20*, also agrees with the structure of bdmac. The two methylene groups in the molecule are observed as negative signals, the two methyl groups (group 1) are observed as one signal at δ39.2, and the remaining nine signals reflect the number of CH groups in the molecule.

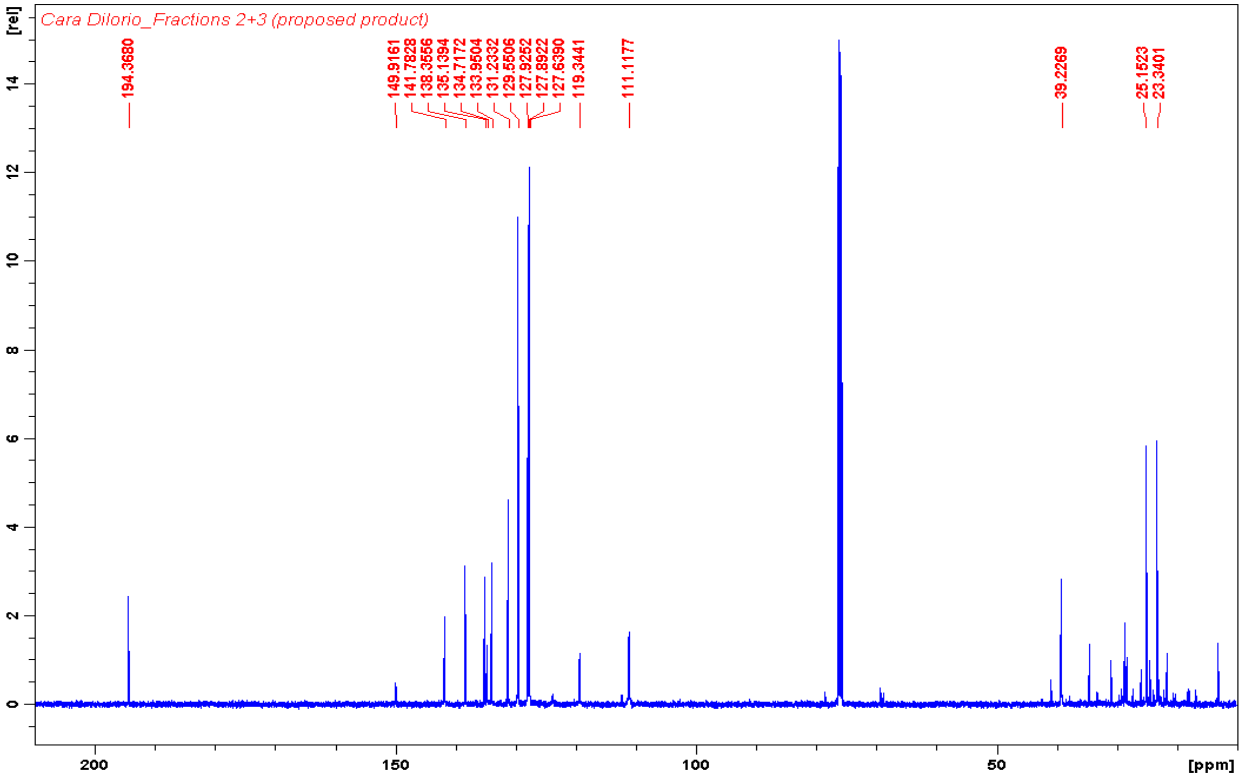

Figure 16: ^{13}C NMR spectrum of bdmac, δ10 – 210 ppm

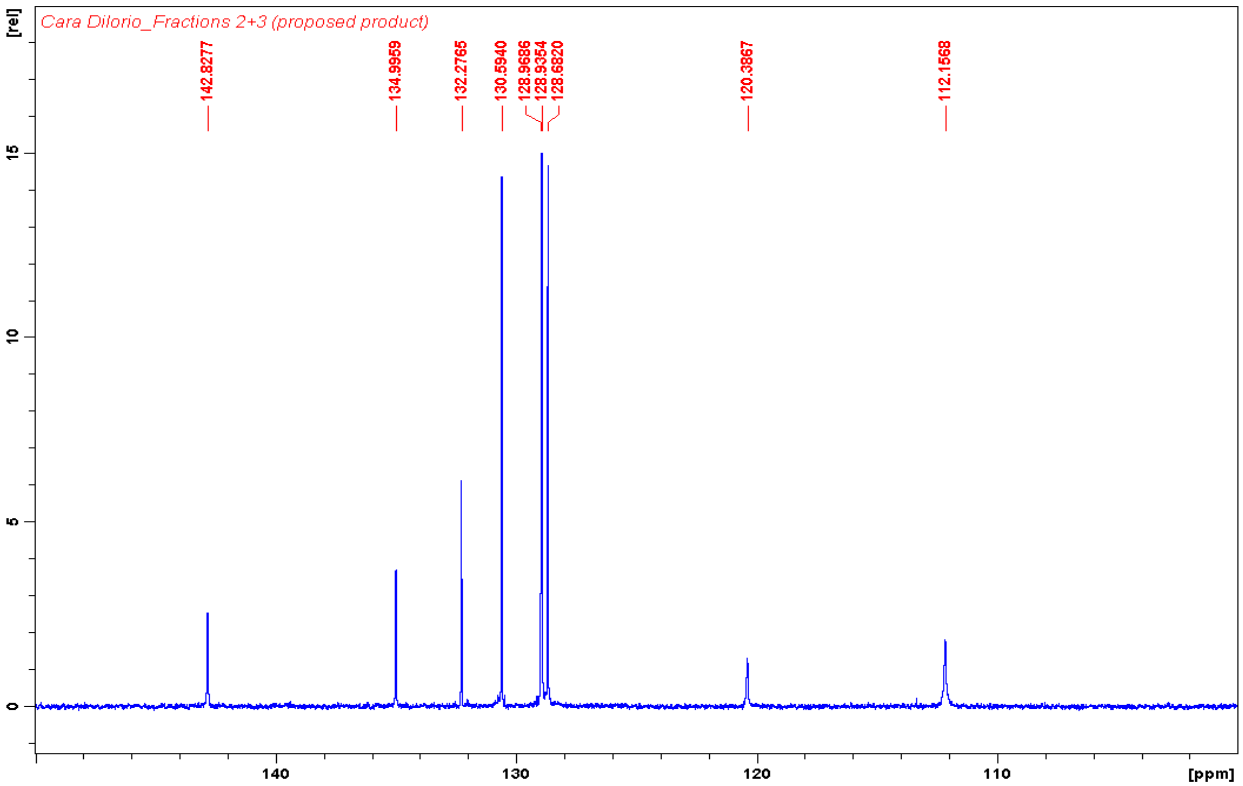

Figure 17: ^{13}C DEPT-90 NMR spectrum of bdmac, δ100 – 150 ppm

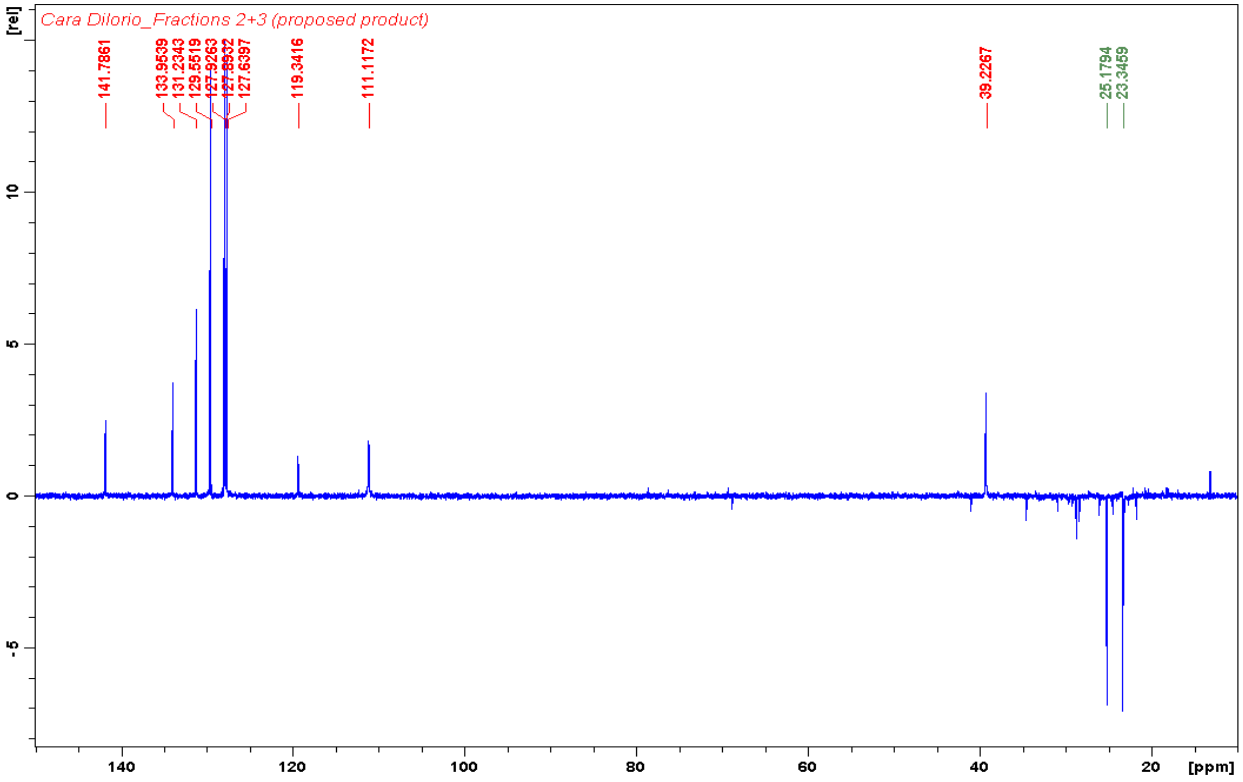

Figure 18: ^{13}C DEPT-135 NMR spectrum of bdmac, δ10 – 150 ppm

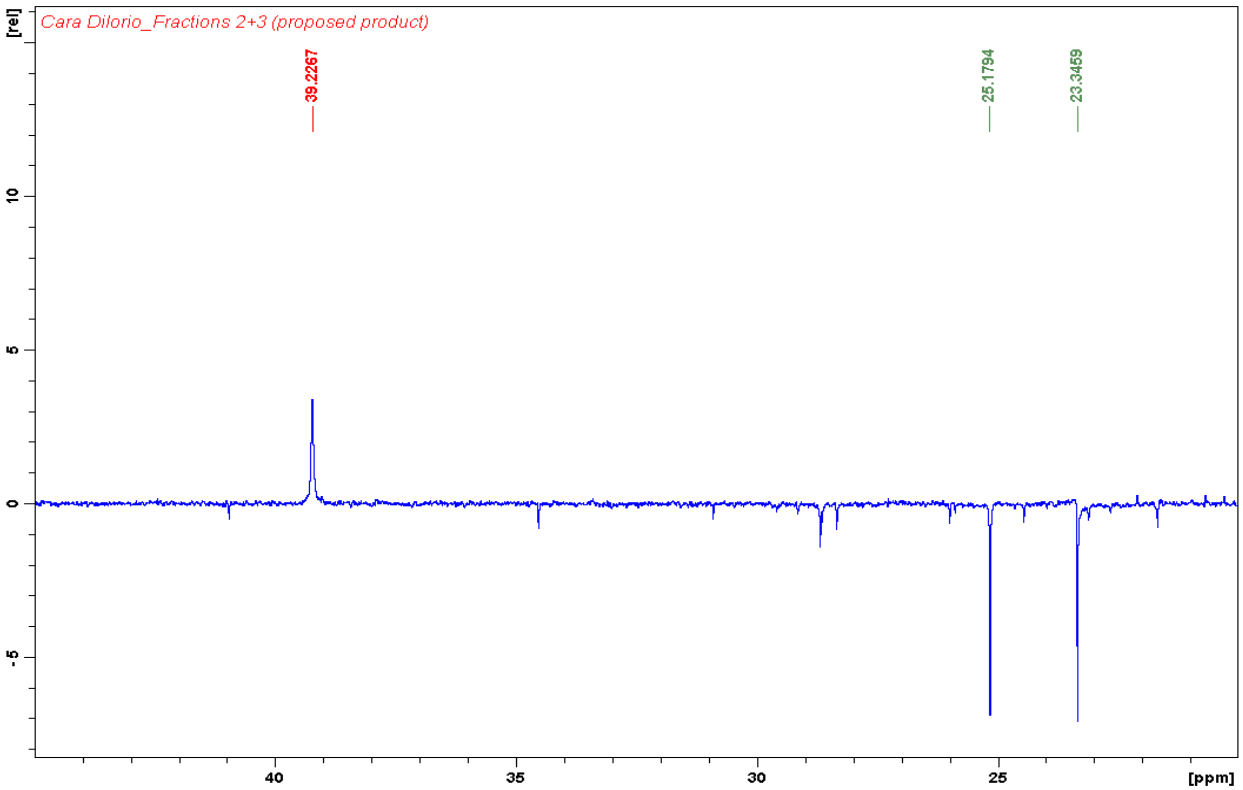

Figure 19: ^{13}C DEPT-135 NMR spectrum of bdmac, δ20 – 45 ppm

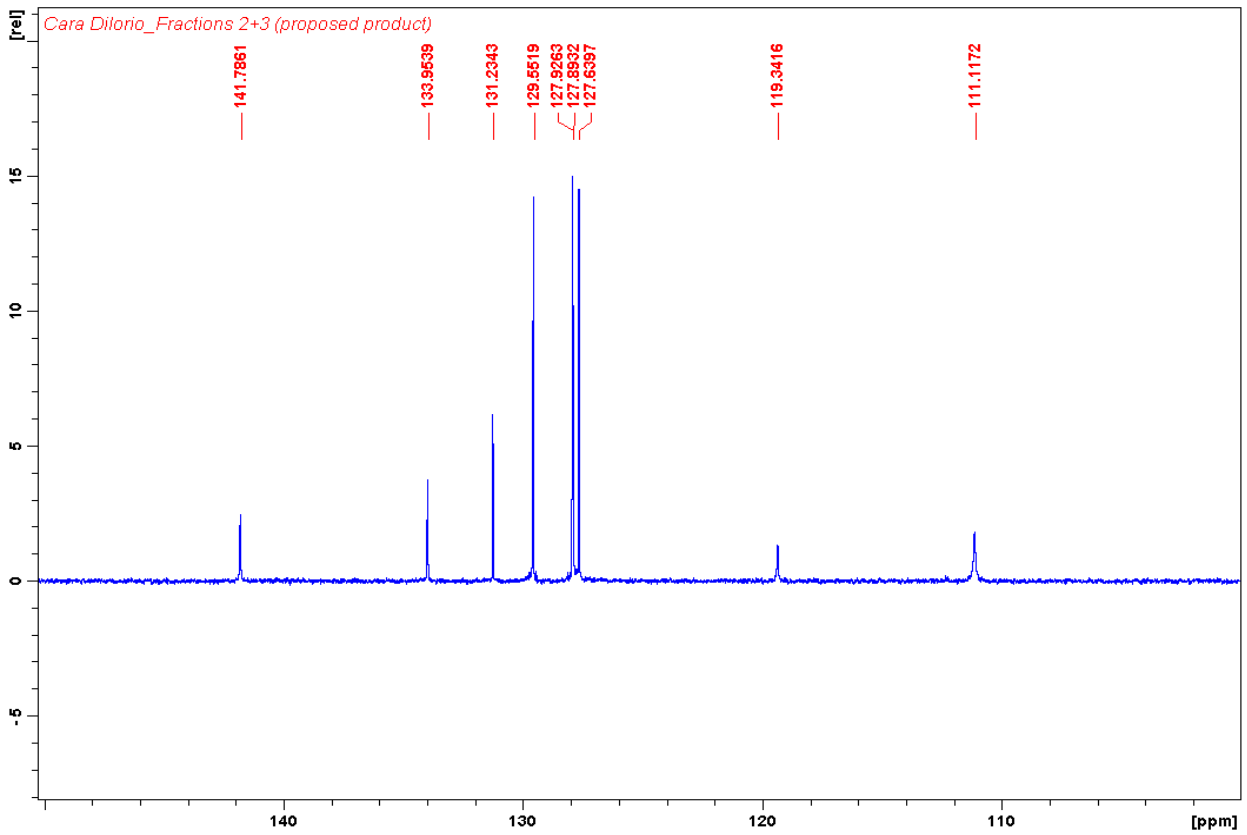

Figure 20: ^{13}C DEPT-135 NMR spectrum of bdmac, δ100 – 150 ppm

Table 1: ^{1}H NMR and ^{13}C NMR spectral data for 1pdbun and bdmac

Compound	^{1}H NMR	^{13}C NMR	^{13}C DEPT-90 NMR	^{13}C DEPT-135 NMR
	δ (ppm)	δ (ppm)	δ (ppm)	δ (ppm)
1pdbun	7.39 (d, 2H), 7.31 – 7.20 (m, 4H†), 2.81 (td, 2H), 2.24 (t, 2H), 1.86 (p, 2H)	206.7, 135.0, 134.4, 131.0, 129.4, 128.2, 127.6, 36.6, 28.2, 19.0	Experiment not performed	Experiment not performed
bdmac	7.49 (d, 2H), 7.40 (t, 1H), 7.34 – 7.30 (m, 4H), 7.27 – 7.24 (m, 2H), 6.86 (d, 1H), 6.71 – 6.66 (m, 1H), 6.59 (d, 2H), 2.97 – 2.93 (m, 2H), 2.91 (s, 6H), 2.82 – 2.79 (m, 2H)	194.3, 149.9, 141.7, 138.3, 135.1, 134.7, 133.9, 131.2, 129.5, 127.9, 127.8, 127.6, 119.3, 111.1, 39.2, 25.1, 23.3	142.8, 134.9, 132.2, 130.5, 128.96, 128.93, 128.6, 120.3, 112.1	141.7, 133.9, 131.1, 129.5, 127.9, 127.8, 127.6, 119.3, 111.1, 39.2, 25.1 (down), 23.3 (down)

†The residual $CDCl_3$ solvent peak is found within this multiplet and adds one hydrogen atom, so the multiplet actually corresponds to 5 hydrogens instead of 4. Trace impurities may also be present in this range.

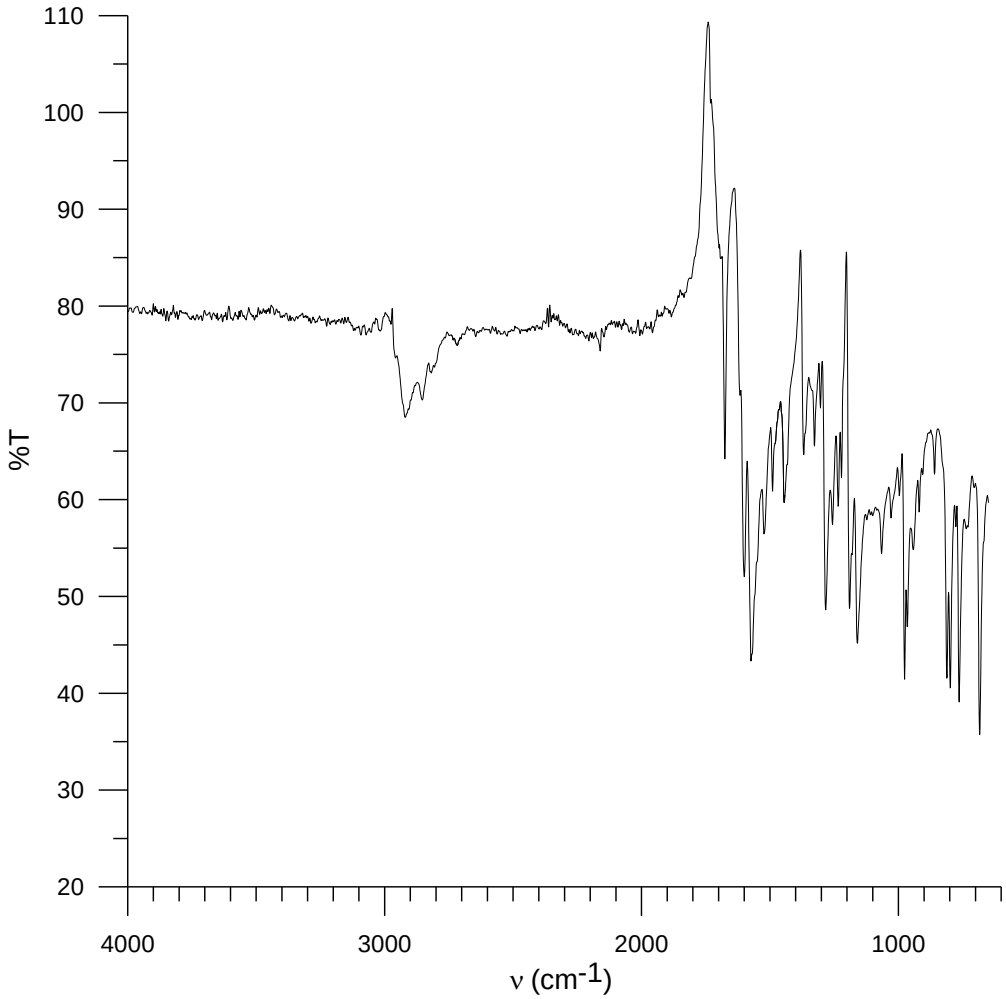

Figure 21: IR spectrum of bdmac

Table 2: IR spectral data for bdmac

Peak (cm^{-1})
2920.65
2853.86
2818.79
1675.97
1600.43
1574.32

The IR peak at 1675.97 cm^{-1} reflects the stretching of the C=O bond in bdmac, while the signals at 1600.43 and 1574.32 cm^{-1} correspond to aromatic C=C bond-stretching. The remaining three signals correspond to the sp^3- and sp^2-hybridized C-H bonds in the molecule.

II. Quantum Chemical Calculations

WPI's WebMO calculator was used to perform quantum chemical calculations on bdmac at the B3LYP/6-311+G(d,p) level of theory. The optimized geometry of the compound was obtained using MOPAC and Gaussian engines. TD-DFT spectral calculations were performed on bdmac in the gas phase and in three solvents (ethanol, dichloromethane, and toluene) using the self-consistent reaction field polarizable continuum model (SCRF PCM). The TD-DFT calculations also provided values for the compound's ground state dipole moment (μ_g) in the gas phase and in each solvent. An additional calculation was performed in order to find the Onsager cavity radius; this value was then used to calculate the change in dipole moment between the excited and ground states ($\Delta\mu$). The excited state dipole moment (μ_e) was obtained from the values of μ_g and $\Delta\mu$.

III. Absorbance and Fluorescence Spectroscopy

Absorbance spectra were obtained on a PerkinElmer® Lambda35 UV/Vis spectrometer, and a PerkinElmer® LS50B fluorescence spectrometer was used to acquire fluorescence spectra. The absorbance and fluorescence characteristics of bdmac were observed in twelve polar protic, polar aprotic, and nonpolar organic solvents. These solvents are presented in *Table 3* according to polarity. In order to determine whether the compound undergoes excited state proton transfer, absorbance and fluorescence spectra in glacial acetic acid were obtained. Based on visual observations of extremely low energy (red) emission of bdmac in frozen methylcyclohexane, it was also hypothesized that bdmac exhibits phosphorescence. Absorbance and fluorescence spectra of bdmac in methylcyclohexane were obtained at room temperature, but time constraints prevented the collection of spectra at 77 K. In order to test this hypothesis in the future, these spectra should be obtained.

Table 3: Organic solvents used in absorbance and fluorescence spectroscopy experiments

Polar protic	Methanol	**Polar aprotic**	Acetonitrile	**Nonpolar**	Toluene
	Ethanol		Dimethylformamide		Carbon disulfide
	1-propanol		Dichloromethane		Carbon tetrachloride
	Isopropanol		Ethyl acetate		n-hexane

IV. Fluorescence Quantum Yields

The fluorescence quantum yield of a compound is defined as the proportion of photons emitted via fluorescence to the amount of photons absorbed by the compound. Fluorescence quantum yields of bdmac were calculated using a comparative method according to the following equation:

$$\Phi_c = \Phi_s \left(\frac{A_s}{A_c} \times \frac{D_c}{D_s} \times \frac{n_c^2}{n_s^2} \right)$$

The fluorescence quantum yield of the standard, or Φ_s, is obtained from the literature. A is the absorbance value at a fixed excitation wavelength; n is the refractive index of the solvents used and is gathered from the literature; and D is the calculated area under the corrected emission spectrum. The subscripts c and s refer to the compound of interest and the standard, respectively.

A set of correction factors was determined in order to correct the fluorescence emission spectra for instrument response. The literature emission spectrum of N,N-dimethylamino-3-nitrobenzene (N,N-DMANB) was compared to its experimental emission spectrum obtained from the LS50B spectrometer utilized in these experiments. Scale factors were then determined every 50 cm^{-1} between 12,500 and 22,200 cm^{-1}.

Fluorescein, which has a published quantum yield of 0.95, was used as the standard for these experiments. A stock solution of fluorescein in 0.1 M NaOH was prepared so that the absorbance maximum was approximately 0.5. The stock solution was then accurately diluted tenfold in order to give a solution with a maximum absorbance of 0.05. The fluorescence

emission spectrum of the diluted standard solution was obtained, fixing the excitation wavelength at λ = 470 nm. The same procedure was followed for bdmac in each solvent studied.

The experimental emission spectral data for bdmac and fluorescein were imported into Microsoft Excel® in order to convert the data from wavelength to wavenumbers. The converted data was then imported into Mathcad®, which was used to correct the emission spectra and calculate quantum yields. *Appendix A* provides a sample quantum yield calculation. Quantum yields of bdmac were determined in methanol, ethanol, isopropanol, acetonitrile, dimethylformamide, dichloromethane, ethyl acetate, toluene, and carbon tetrachloride.

V. Fluorescence Lifetimes

The fluorescence lifetime of a compound (τ_f) is defined as the inverse of the sum of the compound's S_1 first-order radiative (k_f) and non-radiative (k_{nr}) rates of decay according to the following equation:

$$\tau_f = 1/(k_f + k_{nr})$$

Here, k_{nr} is defined as the sum of the rates of internal conversion (k_{ic}) and intersystem crossing (k_{isc}). Fluorescence lifetimes of bdmac were measured using a Photon Technology International® TM-3 Fluorescence Lifetime Spectrometer with a GL-3300 nitrogen laser and GL-302 dye laser.

Solutions of bdmac with a maximum absorbance of approximately 0.05 were prepared using a PerkinElmer® Lambda 35 UV/Vis spectrometer. The solutions were then degassed with nitrogen for 15 minutes in order to prevent fluorescence quenching by oxygen. FeliX-32 computer software was used to generate the time-dependent fluorescence decay spectra of the compound and the instrument response function (IRF). The IRF, or light scatterer, corresponds to the lower limit of the sample lifetime. Ludox®, a 30% weight suspension of colloidal silica, was used as the IRF in these experiments. Neutral density filters were used to adjust the fluorescence intensity of the IRF decay curve.

In order to analyze the data, the decay curve of the sample was fitted to a field fit curve. Best-fit curves were chosen using statistical analysis that determined how well the field fit curve fitted the sample decay curve. *Appendix B* provides a sample fluorescence lifetime calculation. Fluorescence lifetimes of bdmac were determined in ethanol, dichloromethane, and toluene.

VI. Flash Photolysis Studies

The laser flash photolysis (LFP) system used in these experiments is equipped with a 532-nm-wavelength laser and was constructed at Gateway Park in 2012 [2]. In order to confirm that the system was functioning properly, flash photolysis studies were first conducted on tetraphenylporphyrin (TPP) in toluene. Solutions of bdmac in ethanol and toluene were also studied. Samples were prepared so that the absorbance at $\lambda = 532$ nm was approximately 0.3. Samples were excited with the laser and then excited again to a higher-energy triplet state after intersystem crossing was allowed to occur. Although several excitation wavelengths were tested, triplet decay curves of bdmac could not be generated, possibly due to photochemical reactions.

VII. Photochemistry Studies

Photochemistry studies of bdmac were conducted in toluene in an attempt to explain why triplet decay curves could not be generated via laser flash photolysis. A solution of bdmac in toluene was prepared and degassed with nitrogen for approximately 20 minutes, after which an absorbance spectrum was obtained. The solution was then irradiated with a 150 W xenon lamp while continuing to degas with nitrogen. Absorbance spectra were obtained after 15, 30, 45, and 60 minutes of irradiation. The fluorescence spectrum of the 60-minute-irradiated solution was also collected.

Results and Discussion

I. Introduction

The electronic absorbance and fluorescence properties of bdmac were studied in twelve polar protic, polar aprotic, and nonpolar organic solvents. Experimental results show that bdmac exhibits solvatochromism; a bathochromic shift is observed in both absorbance and fluorescence maxima with increasing solvent polarity. Solution color ranged from greenish yellow in nonpolar solvents to reddish orange in alcohols, demonstrating that in the case of bdmac, solvent polarity has an effect on light absorption. Bdmac does not show excited state proton transfer in glacial acetic acid.

Photophysical properties, including fluorescence quantum yields and lifetimes, were also determined in various solvents. Quantum yields ranged from 0.0345 in carbon tetrachloride to 0.4485 in dichloromethane. It was found that quantum yields in nonpolar solvents and alcohols were both low, and the highest quantum yields were observed in polar aprotic solvents. First-order radiative and non-radiative rates of decay of bdmac in ethanol, dichloromethane, and toluene were calculated from fluorescence quantum yields and lifetimes. Although flash photolysis studies were attempted, triplet decay curves for bdmac could not be generated. Photochemistry studies of bdmac in toluene revealed the occurrence of photochemical processes as a result of irradiation.

In addition, quantum chemical calculations were performed on bdmac at the B3LYP/6-311+G(d,p) level of theory. These calculations included geometry optimization in the gas phase and TD-DFT spectral calculations. Spectral calculations were done in the gas phase, ethanol, dichloromethane, and toluene.

Results from the aforementioned experiments will be compared in this section to data obtained previously for (2E,5E)-2-(p-dimethylaminobenzylidene)-5-(p-dimethylamino-cinnamylidene)-cyclopentanone (Ashrbor), a related compound. Like bdmac, Ashrbor is an

asymmetric 2,5-diarylidene cyclopentanone, and it contains electron-donating dimethylamino groups. The only structural difference between the two compounds is that Ashrbor has a dimethylamino group substituted on the *para* position of the benzylidene moiety, while bdmac's benzylidene end is unsubstituted. *Figure 22* shows the structure of Ashrbor.

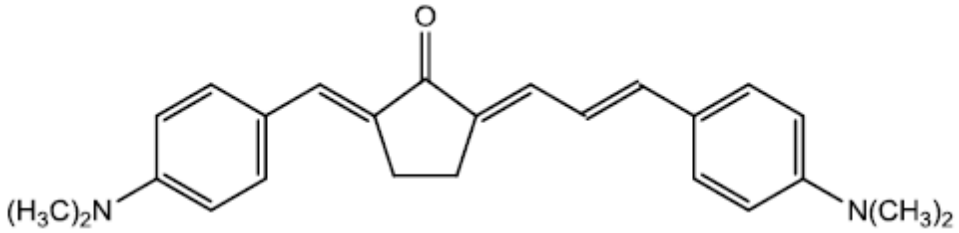

Figure 22: Structure of Ashrbor [15]

II. Quantum Chemical Calculations

The calculated optimized geometry of bdmac is shown in *Figure 23*. The molecule is slightly non-planar, as can be seen from the side view presented in *Figure 24*. The non-planarity of the molecule is also apparent from its dihedral angles. The benzylidene moiety has a dihedral angle of -11°, and the cyclopentanone ring has a dihedral angle of 10°.

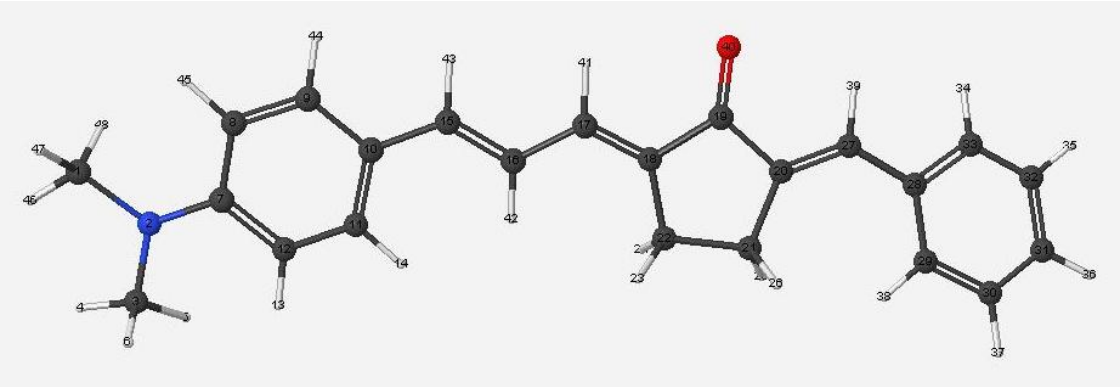

Figure 23: Optimized geometry of bdmac

Figure 24: Side view of bdmac structure showing non-planar geometry

Figure 25 shows the calculated molecular orbitals 86 – 89 in the gas phase. The HOMO-2 (MO 86) is a non-bonding orbital with electron density localized mainly on the cyclopentanone ring and carbonyl oxygen. In the π-bonding HOMO-1 (MO 87), electron density is concentrated on the molecule's benzylidene end. In contrast, electron density is localized on the dimethylaminocinnamylidene end in the HOMO (MO 88), which is also π-bonding. In the π*-antibonding LUMO (MO 89), electron density is primarily centralized on the cyclopentanone ring and carbonyl oxygen, like MO 86.

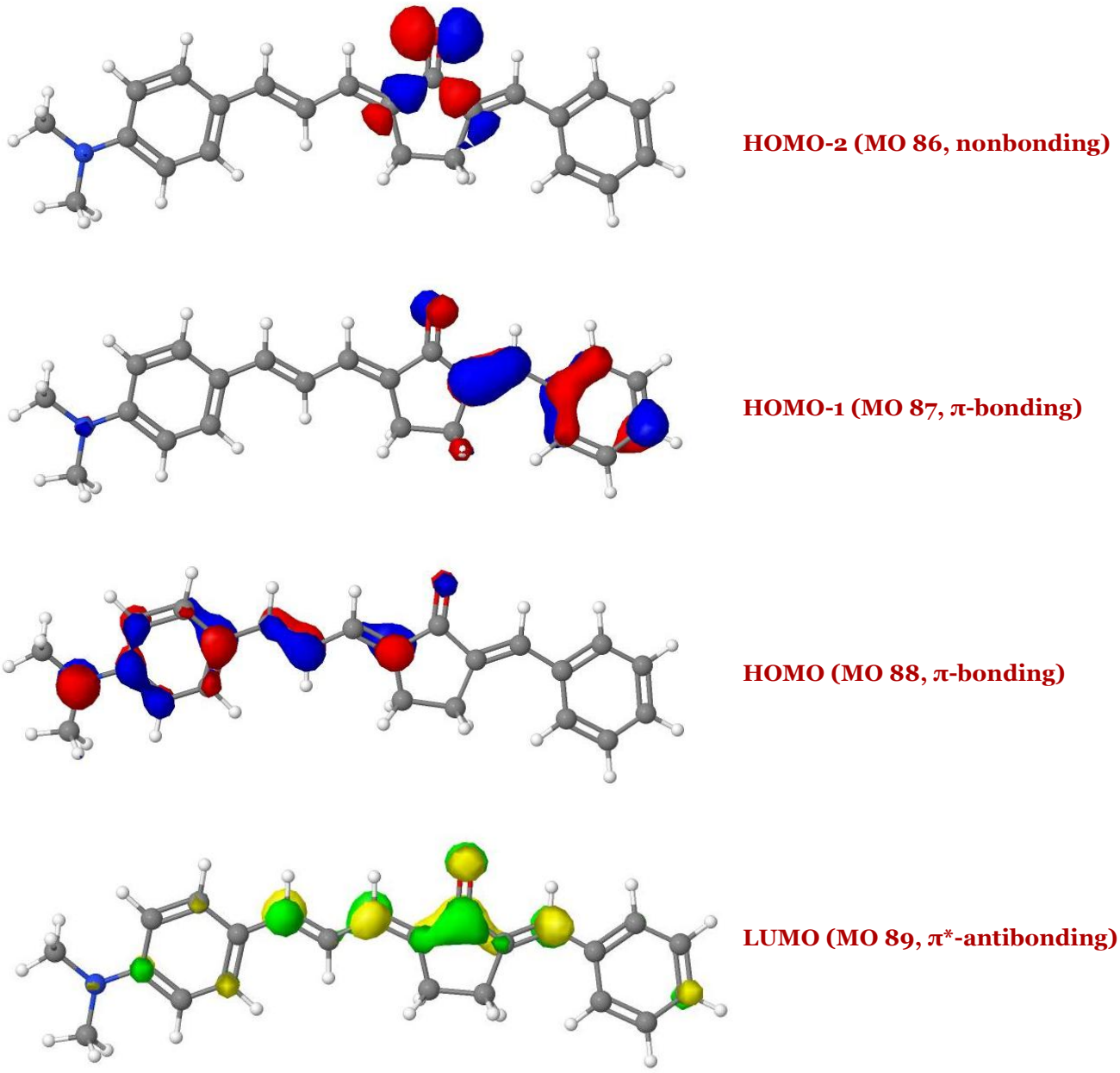

Figure 25: Gas-phase molecular orbitals of bdmac

Table 4 shows the calculated TD-DFT spectral data for bdmac in the gas phase, ethanol, dichloromethane, and toluene. In the gas phase, the most strongly observed transition is S_1, which involves the HOMO and LUMO. As can be seen from *Figure 25*, an internal charge transfer appears to occur upon excitation to the S_1 excited state. Electron density shifts from the electron donor end of the molecule to the electron acceptor end (the carbonyl oxygen) in S_1. The

S_3 transition is the next most strongly observed. The S_2 transition is (n, π*) and only weakly observed, as shown by its low oscillator strength compared to the other two transitions.

The most strongly observed transitions in the solvents are S_1 and S_3, similar to what was observed in the gas phase. In addition, S_1 and S_3 are (π, π*), and S_2 is (n, π*) in all three solvents. However, the latter transition is between MOs 85 and 89 in the solvents and between MOs 86 and 89 in the gas phase. It appears that in solvents, MO 85 is nonbonding and MO 86 is π-bonding, while the opposite is observed in the gas phase.

These calculations show a theoretical bathochromic shift of S_1 and T_1 absorbance maxima of bdmac with increasing solvent polarity. The computed ground state dipole moment, μ_g, also increases as solvent polarity increases. This increase indicates that bdmac interacts more strongly with polar solvents than nonpolar solvents, which explains the calculated bathochromic shift in absorbance maxima with increasing solvent polarity.

Table 4: TD-DFT Spectral Calculations for bdmac

Solvent	Transition	Transition energy			f	CI	MO
		eV	*λ (nm)*	*ν (cm^{-1})*			
Gas (μ_g = 7.53 D)	T_1 (π, π*)	0.61334	761	13149	0	0.64286	88-89
	T_2 (π, π*)	0.42802	531	18841	0	0.59972	87-89
	T_3 (n, π*)	0.38714	480	20831	0	0.66833	86-89
	S_1 (π, π*)	0.37379	464	21573	1.3250	0.70135	88-89
	S_2 (n, π*)	0.34502	428	23374	0.0036	0.66959	86-89
	T_4 (π, π*)	0.34103	423	23647	0	0.50571	85-89
	T_5 (π, π*)	0.32633	405	24713	0	0.49439	88-90
	S_3 (π, π*)	0.28835	358	27968	0.4140	0.62761	87-89
	S_4 (π, π*)	0.26366	327	30587	0.1174	0.61177	88-90
	S_5 (π, π*)	0.25476	316	31656	0.0327	0.66639	85-89
Toluene (μ_g = 8.89 D)	T_1 (π, π*)	1.6004	775	12908	0	0.64596	88-89
	T_2 (π, π*)	2.3493	528	18948	0	0.58387	87-89
	S_1 (π, π*)	2.4499	506	19760	1.5113	0.70357	88-89
	T_3 (n, π*)	2.6979	460	21759	0	0.56839	85-89
	T_4 (π, π*)	2.8728	432	23170	0	0.45663	86-89
	T_5 (π, π*)	2.9798	416	24033	0	0.58547	88-90

	S_2 (n, π*)	3.0028	413	24219	0.0036	0.57945	85-89
	S_3 (π, π*)	3.3856	366	27307	0.4799	0.64906	87-89
	S_4 (π, π*)	3.593	345	28980	0.1048	0.64921	88-90
	S_5 (π. π*)	3.6764	337	29652	0.0171	0.58242	86-89
Dichloromethane (μ_g = 10.09 D)	T_1 (π, π*)	1.5663	792	12633	0	0.65078	88-89
	T_2 (π, π*)	2.3547	527	18992	0	0.57039	87-89
	S_1 (π, π*)	2.3829	520	19219	1.4799	0.70433	88-89
	T_3 (π, π*)	2.7783	446	22409	0	0.45874	86-89
	T_4 (n, π*)	2.8192	440	22739	0	0.51687	85-89
	T_5 (π, π*)	2.9358	422	23678	0	0.60727	88-90
	S_2 (n, π*)	3.0909	401	24930	0.0055	0.66703	85-89
	S_3 (π, π*)	3.3538	370	27050	0.5358	0.64208	87-89
	S_4 (π, π*)	3.6077	344	29098	0.0917	0.64221	88-90
	S_5 (π, π*)	3.6585	339	29508	0.0156	0.66812	86-89
Ethanol (μ_g = 10.46 D)	T_1 (π, π*)	1.5543	798	12537	0	0.65252	88-89
	T_2 (π, π*)	2.3552	526	18996	0	0.56758	87-89
	S_1 (π, π*)	2.3722	523	19133	1.4585	0.7046	88-89
	T_3 (π, π*)	2.7717	447	22355	0	0.5471	86-89
	T_4 (n, π*)	2.8318	438	22840	0	0.65305	85-89
	T_5 (π, π*)	2.9258	424	23598	0	0.6034	88-90
	S_2 (n, π*)	3.1168	398	25138	0.0065	0.67154	85-89
	S_3 (π, π*)	3.3465	370	26991	0.5517	0.63793	87-89
	S_4 (π, π*)	3.6097	343	29115	0.0858	0.63775	88-90
	S_5 (π, π*)	3.66	339	29519	0.0168	0.67144	86-89

The TD-DFT spectral calculations performed on bdmac are presented again in *Table 5* alongside Ashrbor spectral calculations. For both compounds, S_1 is the most strongly observed transition in all solvents, including the gas phase, and it is (π, π*). In the gas phase, S_2 and S_3 are (n, π*) and (π, π*), respectively, for both compounds. However, S_4 and S_5 are both more strongly observed than S_3 in Ashrbor, while the opposite holds true for bdmac. In addition, S_2 is (π, π*) and S_3 is (n, π*) for Ashrbor in all three solvents, but the opposite was observed for bdmac. For Ashrbor in dichloromethane and ethanol, the oscillator strength of the forbidden (n, π*) transition, S_3, is zero. Bdmac's forbidden (n, π *) S_2 transition, on the other hand, is weakly

observed. Except for the S_1 transition, the singlet states of Ashrbor are more red-shifted than those of bdmac. T_1 is also lower in energy for bdmac in all solvents and in the gas phase. Lastly, the calculated S_1 and T_1 transitions become lower in energy with increasing solvent polarity in both compounds.

Table 5: TD-DFT spectral calculations for bdmac and Ashrbor

Solvent	**bdmac**			**Ashrbor**		
	Transition	*λ (nm)*	*f*	*Transition*	*λ (nm)*	*f*
Gas	T_1 (π, π*)	761	0	T_1 (π, π*)	745	0
	T_2 (π, π*)	531	0	T_2 (π, π*)	595	0
	T_3 (n, π*)	480	0	T_3 (n, π*)	482	0
	T_4 (π, π*)	423	0	T_4 (π, π*)	410	0
	T_5 (π, π*)	405	0	T_5 (π, π*)	392	0
	S_1 (π, π*)	464	1.325	S_1 (π, π*)	458	1.7599
	S_2 (n, π*)	428	0.0036	S_2 (n, π*)	427	0.0002
	S_3 (π, π*)	358	0.414	S_3 (π, π*)	403	0.0544
	S_4 (π, π*)	327	0.1174	S_4 (π, π*)	359	0.2355
	S_5 (π, π*)	316	0.0327	S_5 (π, π*)	347	0.1518
Toluene	T_1 (π, π*)	775	0	T_1 (π, π*)	754	0
	T_2 (π, π*)	528	0	T_2 (π, π*)	602	0
	T_3 (n, π*)	460	0	T_3 (n, π*)	461	0
	T_4 (π, π*)	432	0	T_4 (π, π*)	416	0
	T_5 (π, π*)	416	0	T_5 (π, π*)	400	0
	S_1 (π, π*)	506	1.5113	S_1 (π, π*)	495	1.9952
	S_2 (n, π*)	413	0.0036	S_2 (π, π*)	423	0.0485
	S_3 (π, π*)	366	0.4799	S_3 (n, π*)	412	0.0001
	S_4 (π, π*)	345	0.1048	S_4 (π, π*)	363	0.0963
	S_5 (π. π*)	337	0.0171	S_5 (π, π*)	352	0.2417
Dichloromethane	T_1 (π, π*)	792	0	T_1 (π, π*)	765	0
	T_2 (π, π*)	527	0	T_2 (π, π*)	610	0
	T_3 (π, π*)	446	0	T_3 (n, π*)	446	0
	T_4 (n, π*)	440	0	T_4 (π, π*)	424	0
	T_5 (π, π*)	422	0	T_5 (π, π*)	407	0
	S_1 (π, π*)	520	1.4799	S_1 (π, π*)	507	1.9906

	S_2 (n, π*)	401	0.0055	S_2 (π, π*)	431	0.0468
	S_3 (π, π*)	370	0.5358	S_3 (n, π*)	401	0
	S_4 (π, π*)	344	0.0917	S_4 (π, π*)	367	0.1529
	S_5 (π, π*)	339	0.0156	S_5 (π, π*)	355	0.1907
Ethanol	T_1 (π, π*)	798	0	T_1 (π, π*)	769	0
	T_2 (π, π*)	526	0	T_2 (π, π*)	613	0
	T_3 (π, π*)	447	0	T_3 (n, π*)	442	0
	T_4 (n, π*)	438	0	T_4 (π, π*)	427	0
	T_5 (π, π*)	424	0	T_5 (π, π*)	408	0
	S_1 (π, π*)	523	1.4585	S_1 (π, π*)	509	1.9763
	S_2 (n, π*)	398	0.0065	S_2 (π, π*)	433	0.0455
	S_3 (π, π*)	370	0.5517	S_3 (n, π*)	398	0
	S_4 (π, π*)	343	0.0858	S_4 (π, π*)	368	0.2345
	S_5 (π, π*)	339	0.0168	S_5 (π, π*)	356	0.1119

*Note 1: Spectral calculations for Ashrbor were performed at the B3LYP/6-31G(d) level of theory, while spectral calculations for bdmac were performed at the B3LYP/6-311+G(d,p) level of theory.
*Note 2: Ashrbor calculations were performed by Christopher Zoto, Ph.D.

Table 6 compares the calculated ground state dipole moments of bdmac and Ashrbor in the gas phase, toluene, dichloromethane, and ethanol. Bdmac has larger dipole moments than Ashrbor, which is probably a reflection of the structural differences between the two compounds. Ashrbor's second dimethylamino group may lessen the compound's overall dipole moment in comparison to bdmac.

Table 6: Computed ground state dipole moments of bdmac and Ashrbor

Solvent	**μ_g (D)**	
	bdmac	*Ashrbor*
Gas	7.53	5.60
Toluene	8.89	6.57
Dichloromethane	10.09	7.47
Ethanol	10.46	7.76

*Note 1: Ashrbor data taken from [15]

III. Spectroscopic Properties of bdmac

The absorbance and fluorescence spectroscopic properties of bdmac were examined in twelve solvents; *Figure 26* displays the absorbance and uncorrected fluorescence emission spectra of the compound in eight of these solvents. Absorbance maxima ranged from 435 nm (22,988 cm^{-1}) in n-hexane to 481 nm (20,790 cm^{-1}) in methanol, a range of 46 nm. The range of corrected fluorescence maxima is 196 nm; values ranged from 518 nm (19,272 cm^{-1}) in n-hexane to 714 nm (13,996 cm^{-1}) in methanol. These ranges demonstrate a bathochromic shift in both absorbance and fluorescence maxima with increasing solvent polarity and clearly show that this shift is more pronounced in fluorescence maxima than in absorbance maxima. This unequal bathochromic shift can be noted from *Figure 26* as well. The absorbance and emission bands also become broader as solvent polarity increases, and vibronic structure is observed in nonpolar solvents. The range of solution colors observed is displayed in *Figure 27*.

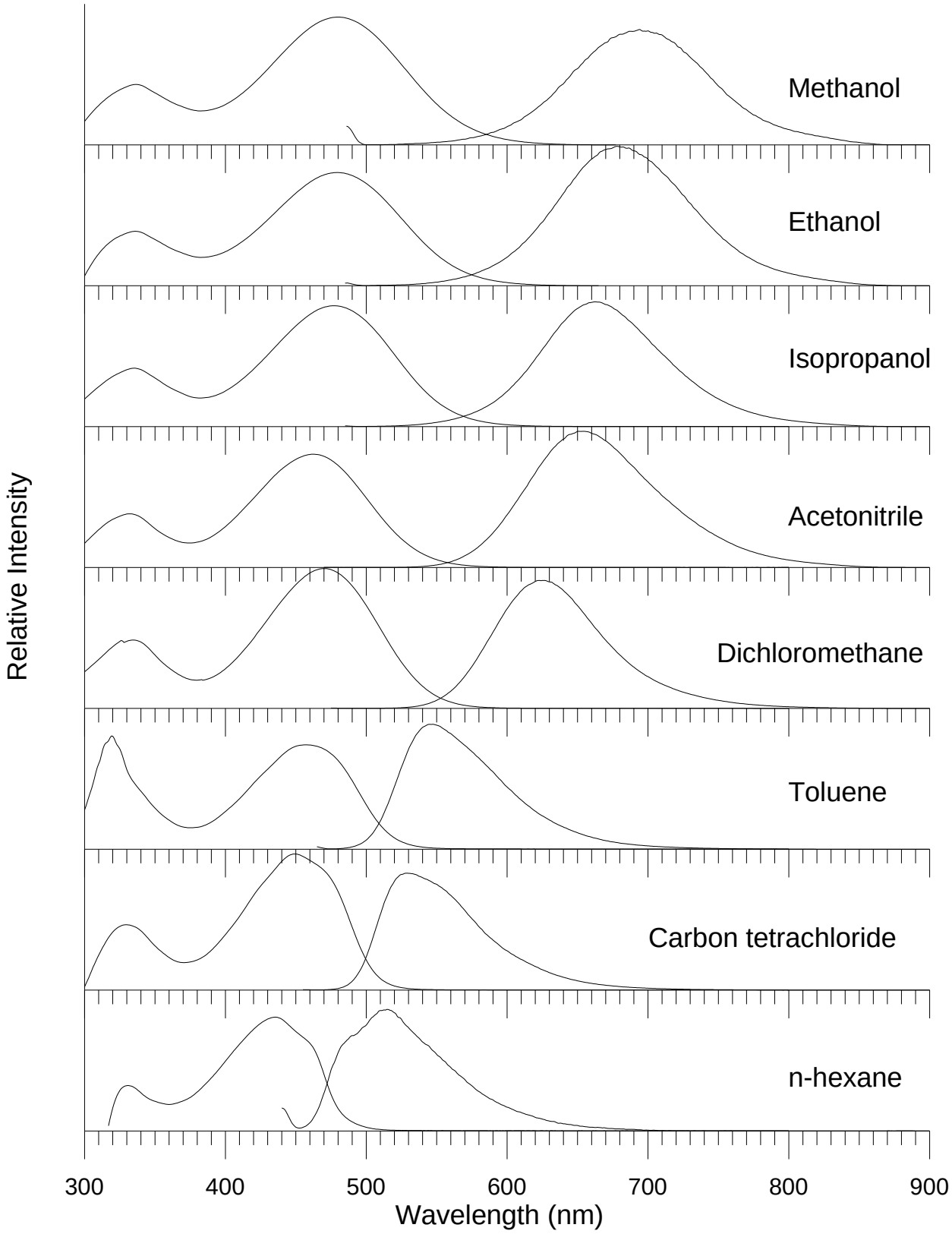

Figure 26: Experimental absorbance and fluorescence spectra of bdmac in various solvents

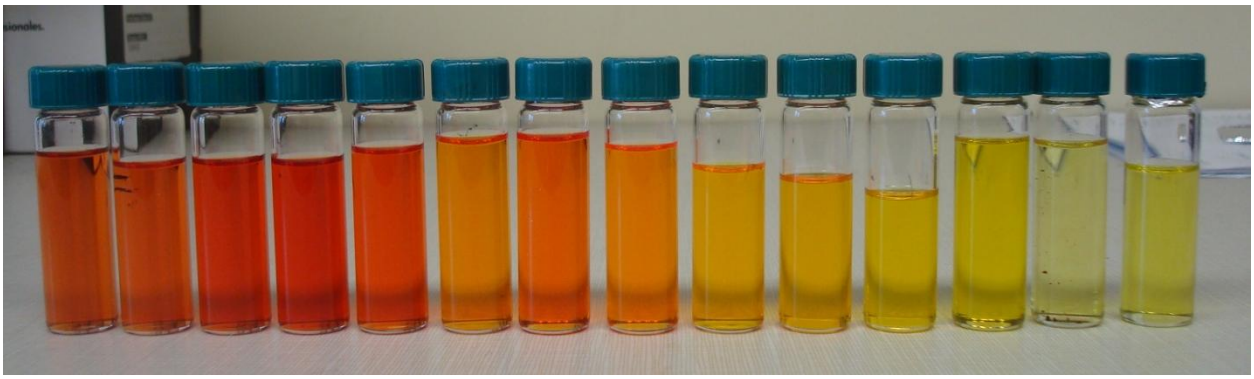

Figure 27: From left to right, solutions of bdmac in HOAc, MeOH, EtOH, 1-PrOH, 2-PrOH, ACN, DMF, DCM, EtOAc, CS_2, Toluene, CCl_4, n-hexane, and methylcyclohexane

Table 7 gives tabulated absorbance and fluorescence spectral data for bdmac in each of the twelve solvents studied, as well as that for glacial acetic acid. It is important to note that the fluorescence data presented here has been corrected in Mathcad®. The solvent polarity function (Δf) and the empirical scale of solvent polarity ($E_T(30)$ scale) are also shown in the table. The $E_T(30)$ empirical scale is a measure of the polarity of a solvent and is based on the charge transfer shift of the first maximum of a betaine dye [13]. The solvent polarity function relates the dielectric constant (ε) and the refractive index (n) of a given solvent [15]. Like the $E_T(30)$ scale, it is a gauge of a solvent's polarity. It is defined as

$$\Delta f = \frac{\varepsilon - 1}{2\varepsilon + 1} - \frac{n^2 - 1}{2n^2 - 1}$$

The Stokes' shift (Δν) is the difference between the fluorescence and absorbance maxima of a compound in wavenumbers. As can be noted from the table, this value generally increases with increasing solvent polarity, showing that fluorescence maxima change more dramatically with increasing solvent polarity than do absorbance maxima. Stokes' shifts ranged from 3716 cm^{-1} in n-hexane to 7347 cm^{-1} in acetonitrile.

Table 7: Experimental absorbance and fluorescence spectral data for bdmac

Solvent	λ_{abs} (nm)	λ_f (nm)	ν_{abs} (cm^{-1})	ν_f (cm^{-1})	$E_T(30)$ (kcal/mol)	Δf	Δν (cm^{-1})
Glacial acetic acid	486	705	20576	14166	---	---	6410
Methanol	481	714	20790	13996	55.4	0.3093	6794
Ethanol	480	704	20833	14187	51.9	0.2887	6646
1-propanol	481	703	20790	14217	50.7	0.2746	6573
Isopropanol	477	701	20964	14248	48.4	0.2769	6716
Acetonitrile	462	699	21645	14298	45.6	0.3054	7347
Dimethylformamide	472	698	21186	14319	43.2	0.2752	6867
Dichloromethane	470	655	21276	15254	40.7	0.2171	6022
Ethyl acetate	453	618	22075	16180	38.1	0.1996	5895
Toluene	457	581	21881	17184	33.9	0.0131	4697
Carbon disulfide	473	583	21141	17141	32.8	-0.0007	4000
Carbon tetrachloride	449	556	22271	17966	32.4	0.0119	4305
n-hexane	435	518	22988	19272	31	-0.0004	3716

*Note 1: $E_T(30)$ and Δf values taken from [15]

Figure 28 relates the absorbance and fluorescence maxima of bdmac in each solvent to the $E_T(30)$ empirical polarity scale. A single trend line was fitted to the absorbance data because a similar trend in absorbance maxima was observed for all solvents. The line has a negative slope, indicating a decrease in ν_{abs} with increasing solvent polarity.

Two separate trend lines were fitted to the fluorescence data because the trend observed among alcohols differed from that observed among the other eight solvents. The slope of both trend lines is negative, so ν_f also decreases with increasing solvent polarity. However, the decrease in ν_f is more dramatic among the non-alcoholic solvents than among alcohols, as the slope of the non-alcohol line is about eight times as steep as that of the alcohol line.

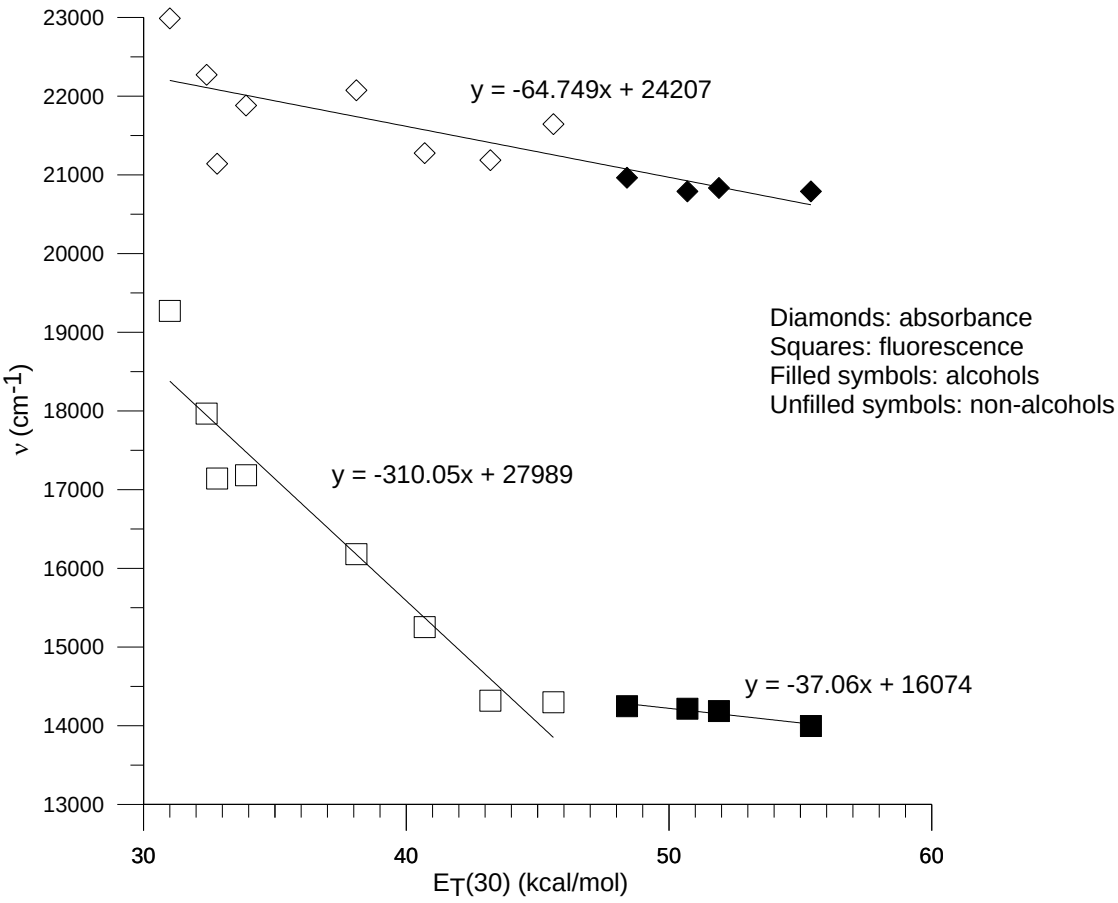

Figure 28: Linear relationship between experimental spectral maxima of bdmac and the $E_T(30)$ scale

Figure 29 is a Lippert-Mataga plot, relating the Stokes' shift of bdmac in all twelve solvents to values of the solvent polarity function. As the figure shows, the Stokes' shift becomes greater with increasing solvent polarity. Based on the trend lines fitted to the data, this increase is more dramatic among non-alcohols than among alcohols.

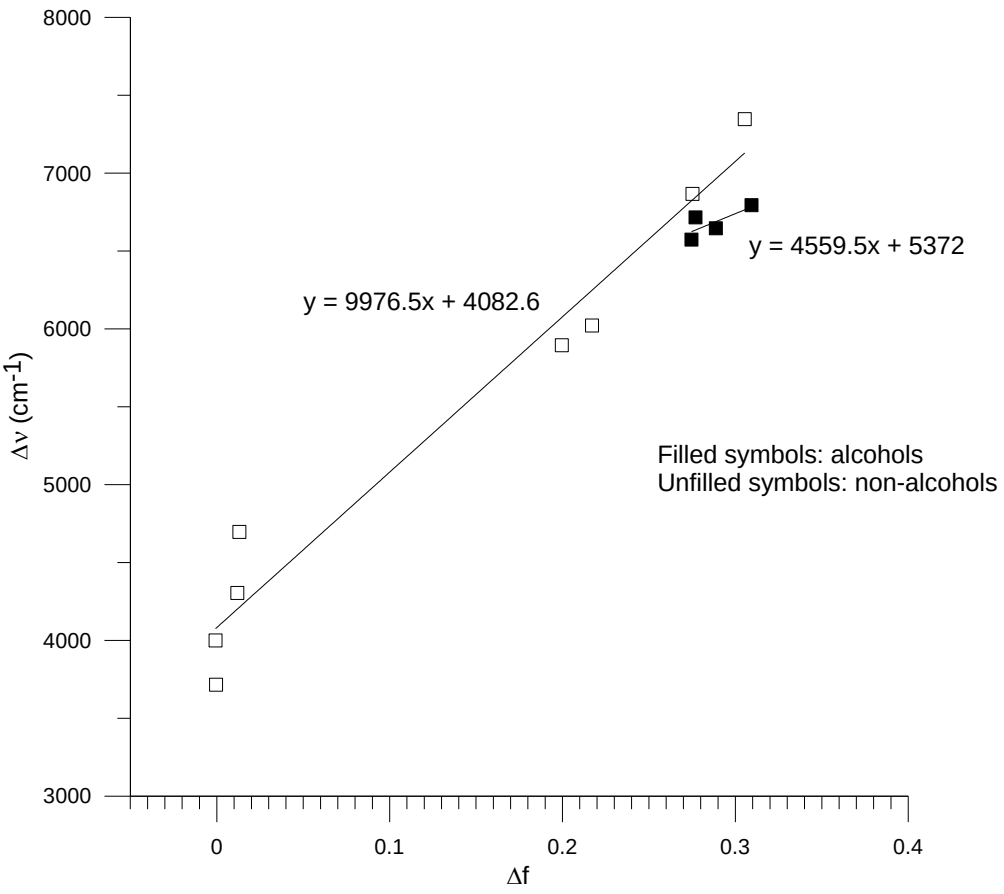

Figure 29: Lippert-Mataga plot of experimental absorbance and fluorescence spectral data for bdmac

The Lippert-Mataga equation is a relation between the Stokes' shift of a compound in a given solvent and the value of the solvent polarity function for that solvent [15]. It is given by

$$\Delta\nu = \frac{2\Delta\mu^2}{hca^3}\Delta f + \text{constant}$$

where $\Delta\mu$ represents the change in dipole moment between the ground and excited states ($\mu_e - \mu_g$); h is Planck's constant; c is the speed of light in a vacuum; and a is the compound's Onsager cavity radius. The equation is in the form y = mx + b, so the slope of a Lippert-Mataga trend line is equivalent to $(2\Delta\mu^2/hca^3)$ and can be used to calculate μ_e. Quantum chemical calculations revealed that the Onsager cavity radius of bdmac is 5.64 A, and μ_g is 7.53 D in the gas phase. Using these two values and the slopes of three trend lines, three different values of μ_e were

obtained. The value of μ_e is 20.4 D for all solvents, 16.5 D for alcohols (protic solvents), and 20.9 D for non-alcohols (aprotic solvents).

Like bdmac, Ashrbor is also a charge transfer compound. Upon excitation from S_0 to S_1, electron density shifts from the electron-donating dimethylamino group(s) to the electron-accepting carbonyl group. Both the change in dipole moment from ground to excited states and the excited state dipole moment of a compound reflect the degree of internal charge transfer that occurs upon excitation. The degree of internal charge transfer is in turn a reflection of the number of electron-donating groups the compound has [15].

The excited state dipole moment of Ashrbor in aprotic solvents was previously calculated to be 21.1 D, with a change of 15.5 D between the ground and excited states [15]. Both of these values are greater than analogous values for bdmac (μ_e = 20.9 D; $\Delta\mu$ = 13.3 D) because Ashrbor has one more electron-donating group than bdmac. This means that the degree of internal charge transfer is greater in Ashrbor than in bdmac.

The spectroscopic data for bdmac is reproduced in *Table 8* alongside analogous data for Ashrbor. In general, the absorbance and fluorescence maxima of both compounds become more red-shifted with increasing solvent polarity. Carbon tetrachloride is an anomaly for Ashrbor, and carbon disulfide is an anomaly for bdmac. The ranges of absorbance and fluorescence maxima for Ashrbor are 51 nm and 222 nm, respectively. Both shifts are somewhat greater than the shifts of bdmac's spectral maxima (46 nm and 196 nm). This could be a result of Ashrbor's extra dimethylamino group.

Absorbance maxima are more red-shifted in Ashrbor than in bdmac, which is another reflection of Ashrbor having more electron-donating groups than bdmac [15]. However, the fluorescence maxima are generally more red-shifted in bdmac. Both compounds exhibit an increase in the Stokes' shift with increasing solvent polarity, and bdmac has greater Stokes' shifts than Ashrbor in all solvents presented. Differences in the value of the Onsager cavity

radius (5.64 A in bdmac and 5.97 A in Ashrbor) explain why bdmac has larger Stokes' shifts but a smaller Δμ than Ashrbor.

Table 8: Experimental absorbance and fluorescence spectral data for bdmac and Ashrbor

Solvent	bdmac					Ashrbor				
	λ_{abs} (nm)	λ_f (nm)	ν_{abs} (cm^{-1})	ν_f (cm^{-1})	$\Delta\nu$ (cm^{-1})	λ_{abs} (nm)	λ_f (nm)	ν_{abs} (cm^{-1})	ν_f (cm^{-1})	$\Delta\nu$ (cm^{-1})
Methanol	481	714	20790	13996	6794	500	737	20000	13570	6430
Ethanol	480	704	20833	14187	6646	498	725	20080	13790	6290
1-propanol	481	703	20790	14217	6573	499	717	20040	13953	6087
Isopropanol	477	701	20964	14248	6716	493	687	20284	14557	5727
Acetonitrile	462	699	21645	14298	7347	478	666	20921	15016	5905
Dimethyl-formamide	472	698	21186	14319	6867	486	656	20576	15237	5339
Dichloromethane	470	655	21276	15254	6022	484	635	20661	15747	4914
Ethyl acetate	453	618	22075	16180	5895	464	591	21552	16920	4632
Toluene	457	581	21881	17184	4697	475	532	21053	18807	2246
Carbon disulfide	473	583	21141	17141	4000	475	530	21053	18858	2195
Carbon tetrachloride	449	556	22271	17966	4305	489	540	20450	18518	1932
n-hexane	435	518	22988	19272	3716	449	515	22272	19402	2870

*Note 1: Ashrbor data taken from [15]

Figure 30 shows the experimental absorbance and fluorescence emission spectra of bdmac and Ashrbor in glacial acetic acid (Ashrbor spectra were collected by Christopher Zoto, Ph.D.). The objective of this experiment was to investigate a novel application of 2,5-diarylidene cyclopentanones: use as pH probes. If these molecules exhibit excited state proton transfer in glacial acetic acid, two emission bands are observed in the fluorescence spectrum. It was hypothesized that the ratio of the emission intensities of the two bands could be related to the pH of the acid.

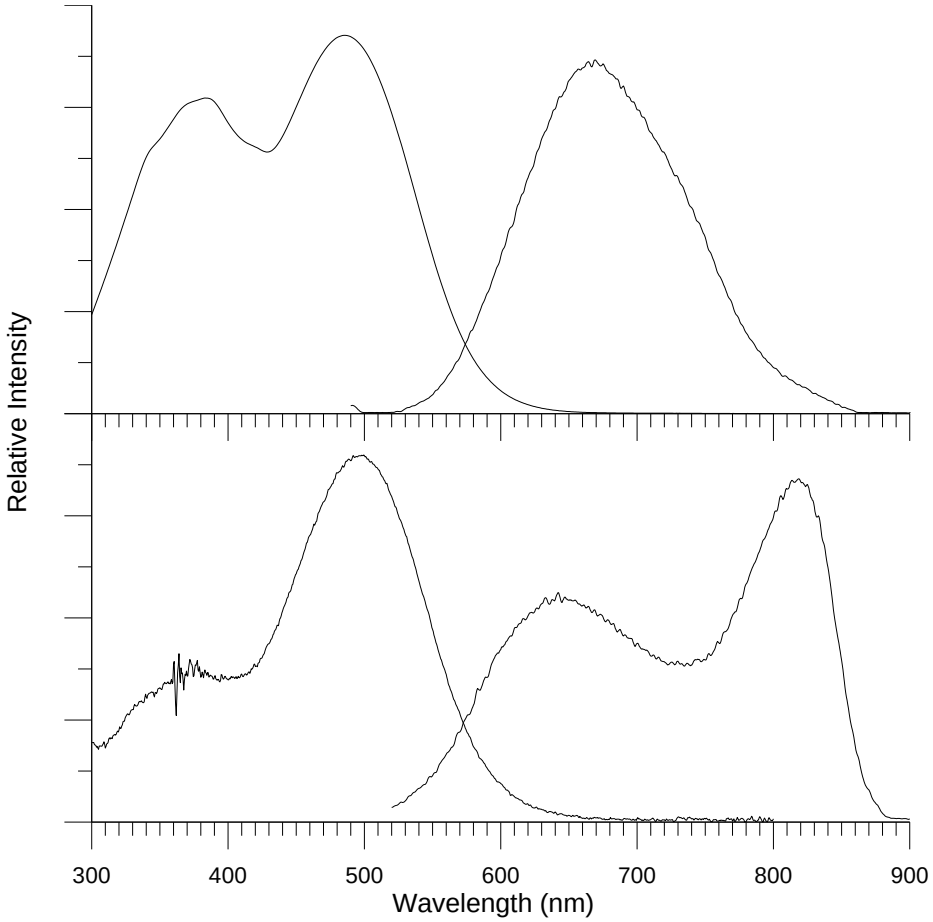

Figure 30: Experimental absorbance and fluorescence spectra of bdmac (top) and Ashrbor (bottom) in glacial acetic acid

However, bdmac was not found to exhibit excited state protonation in concentrated glacial acetic acid, as evidenced by the absence of a second, lower-energy emission band in its fluorescence spectrum. The observed emission band (699 nm) follows the trend of fluorescence maxima of bdmac in other solvents and probably corresponds to unprotonated emission from S_1.

The compound is not likely to exhibit ground state protonation either; the absorbance peak at 486 nm (the lower-energy band in the figure) follows the trend of absorbance maxima of bdmac in other solvents and appears to be the S_1 transition. Therefore, the higher-energy absorbance band is probably the S_3 transition. If bdmac exhibited ground state protonation, the corresponding peak would be lower in energy than the S_1 band, but no such peak is observed.

Ashrbor, on the other hand, does exhibit excited state protonation. Two emission bands, one at 642 nm and the other at 818 nm, are observed in its fluorescence spectrum in concentrated glacial acetic acid. The higher-energy band follows the trend of fluorescence maxima of Ashrbor in other solvents and corresponds to unprotonated S_1 emission, while the lower-energy band corresponds to protonated S_1 emission. This indicates that a proportion of the molecules become protonated upon excitation to S_1 and before emission. Future work with Ashrbor should involve obtaining absorbance and fluorescence spectra of the compound in acids of varying pH. If the ratio between the two emission bands correlates to the pH of the acid, Ashrbor could be used as a pH probe.

Atomic partial charge calculations were performed on bdmac and Ashrbor in an attempt to explain the observations from the above experiment. It was found that the change in charge on the carbonyl oxygen between S_1 and S_0 is −0.07232 in bdmac and −0.07748 in Ashrbor, a difference of ~0.005. This indicates a slightly higher degree of internal charge transfer in Ashrbor than in bdmac upon excitation to S_1, which makes Ashrbor a stronger base than bdmac in the excited state. Ashrbor is therefore more likely than bdmac to undergo excited state proton transfer in acid. Higher-order calculations should be performed in the future in order to obtain more accurate atomic partial charges.

Figure 31 shows the experimental room-temperature absorbance and fluorescence emission spectra of bdmac in methylcyclohexane. Prominent vibronic structure is observed in both spectra. The major peak in the absorbance spectrum corresponds to the 0-1 excitation from S_0 to S_1, while the lower-energy shoulder probably corresponds to the 0-0 excitation from S_0 to S_1. The higher-energy S_3 band is also observed. In the fluorescence spectrum, three bands are observed. The lower-energy shoulder on the major peak corresponds to the 2-0 emission from S_1 to S_0, while the higher-energy peak corresponds to the 0-0 emission from S_1 to S_0. The major peak reflects the 1-0 emission from S_1. In the future, spectra should also be obtained at 77 K to

determine whether bdmac exhibits phosphorescence in methylcyclohexane. Evidence of phosphorescence has not been reported for any other 2,5-diarylidene cyclopentanone.

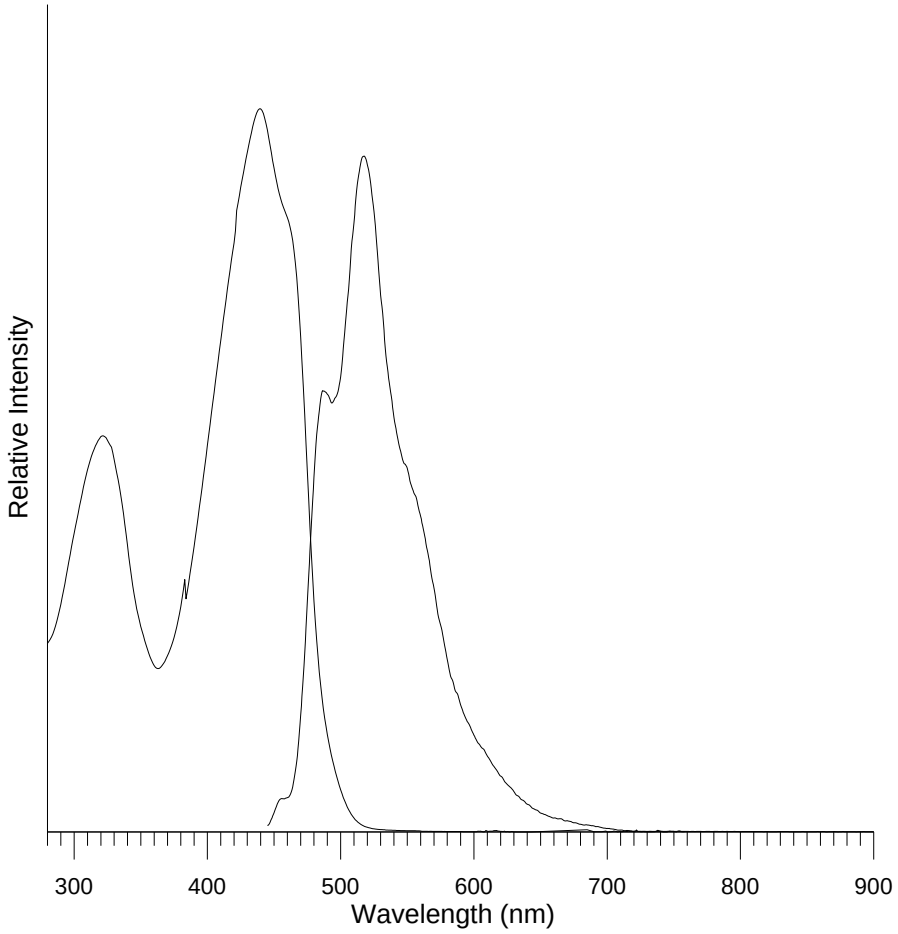

Figure 31: Experimental room-temperature absorbance and fluorescence spectra of bdmac in methylcyclohexane

IV. Photophysical Properties of bdmac

Table 9 displays the photophysical properties of bdmac in various solvents. Fluorescence quantum yields, lifetimes, and decay constants were experimentally determined, and energy gaps were obtained computationally. Quantum yields were measured in nine solvents, while time constraints limited the study of fluorescence lifetimes and (π, π^*) → (n, π^*) energy gaps to three solvents: ethanol, dichloromethane, and toluene. First-order radiative and non-radiative

rates of decay in these three solvents were calculated from quantum yield and lifetime data according to the following equations:

$$k_f = \frac{\Phi_f}{\tau_f}$$

$$k_{nr} = \left(\frac{1}{\Phi_f} - 1\right) k_f$$

For the quantum yield experiments, two samples were studied per solvent to ensure reproducibility of results; average quantum yield values are presented in the table. The highest quantum yields were observed for the four polar aprotic solvents. The alcohols and nonpolar solvents studied showed similar quantum yields. Quantum yields ranged from 0.0345 in carbon tetrachloride to 0.4485 in dichloromethane.

Computed energy gaps between the lowest lying (π, π*) and (n, π*) states were found to increase with increasing solvent polarity for both singlet and triplet multiplicities. Lifetimes roughly correlated with quantum yields, and k_{nr} values appear to be inversely related to quantum yields.

Table 9: Experimental and computational photophysical properties of bdmac

Solvent	**Φ_f**	**$\Delta E_{(\pi,\pi^*) \rightarrow (n,\pi^*)}$ (cm^{-1})**		**τ_f (ns)**	**k_f (s^{-1})**	**k_{nr} (s^{-1})**
		Singlet	*Triplet*			
Methanol	0.036	---	---	---	---	---
Ethanol	0.117	6005	10303	0.46	2.54×10^8	1.92×10^9
Isopropanol	0.2005	---	---	---	---	---
Acetonitrile	0.3395	---	---	---	---	---
Dimethylformamide	0.43	---	---	---	---	---
Dichloromethane	0.4485	5711	10106	1.85	2.42×10^8	2.98×10^8
Ethyl acetate	0.2205	---	---	---	---	---
Toluene	0.076	4459	8851	0.81	9.38×10^7	1.14×10^9
Carbon tetrachloride	0.035	---	---	---	---	---

Figures 32 – 33 show how the average quantum yields of bdmac in the aforementioned nine solvents relates to fluorescence maxima in wavenumbers and to the $E_T(30)$ empirical scale,

respectively. In both cases, a roughly bell-shaped curve demonstrates the relationship between the two variables. Polar aprotic solvents, which have moderate polarity and medium-energy fluorescence maxima, exhibit the highest quantum yields. Polar protic and nonpolar solvents, on the other hand, both have low quantum yields. Graphs relating k_{nr} values to solvent polarity were not constructed because only three such values were obtained. It will be necessary in the future to measure lifetimes of bdmac in more solvents in order to determine this relationship.

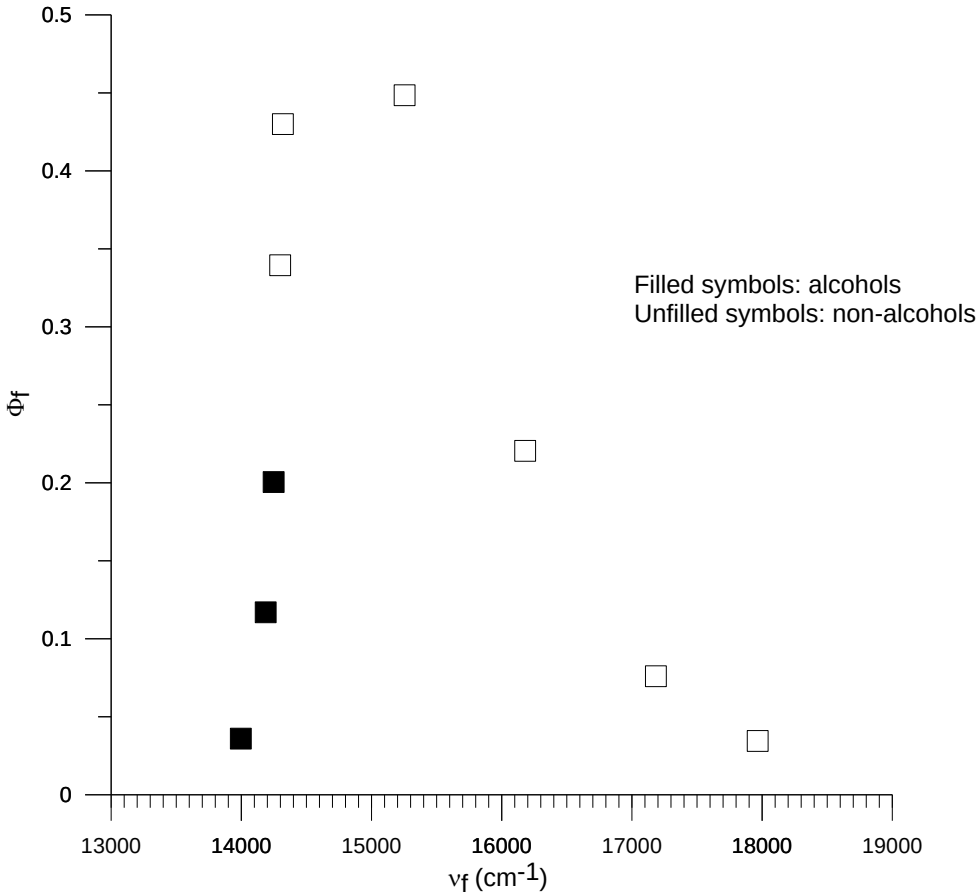

Figure 32: Bell-shaped relationship between experimental fluorescence quantum yields and fluorescence maxima of bdmac

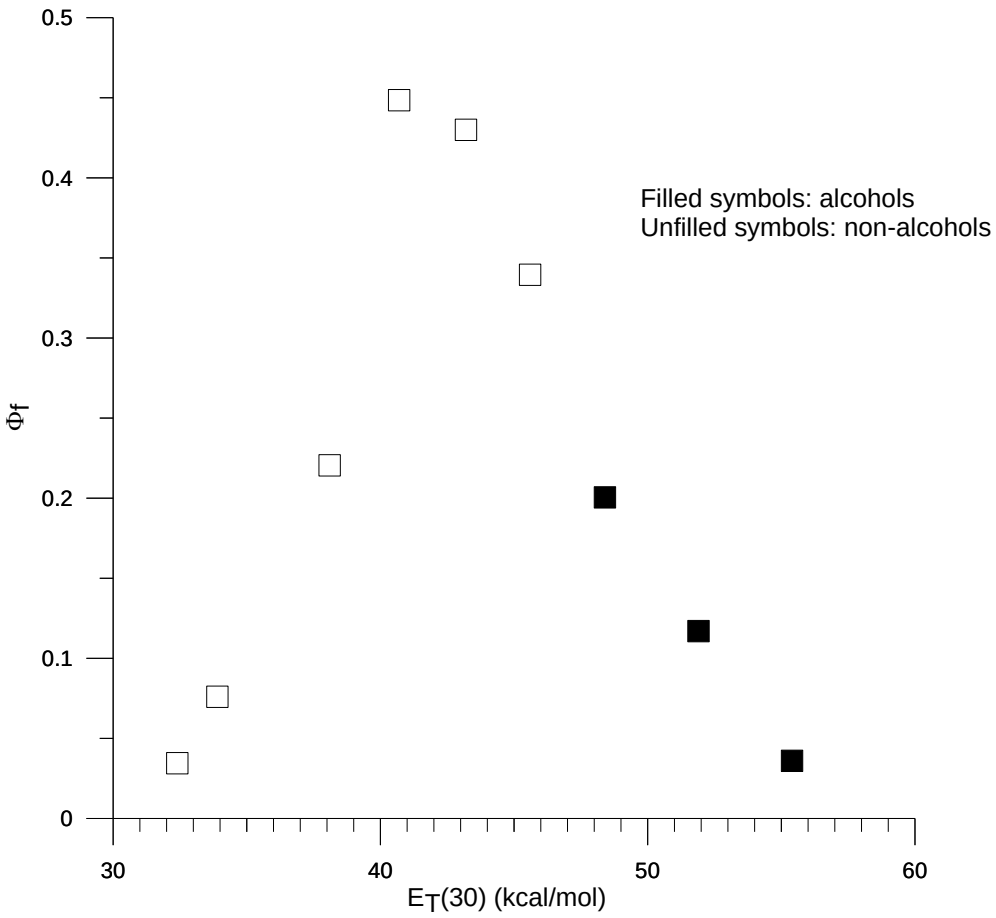

Figure 33: Bell-shaped relationship between experimental fluorescence quantum yields of bdmac and the $E_T(30)$ scale

This observed trend in the quantum yields of bdmac is not unusual among other 2,5-diarylidene cyclopentanones. The reason for the trend has been proposed to involve rates of intersystem crossing and internal conversion, and it relates to El-Sayed's rule, vibronic spin-orbit coupling, and the energy gap rule [14, 15]. El-Sayed's rule states that intersystem crossing between two excited states of differing orbital configurations is more efficient than that between two excited states of the same orbital configuration [15]. In other words,

$$k_{isc}\{^1(\pi, \pi^*) \rightarrow {}^3(n, \pi^*)\} \text{ and } k_{isc}\{^1(n, \pi^*) \rightarrow {}^3(\pi, \pi^*)\} >>>$$

$$k_{isc}\{^1(\pi, \pi^*) \rightarrow {}^3(\pi, \pi^*)\} \text{ and } k_{isc}\{^1(n, \pi^*) \rightarrow {}^3(n, \pi^*)\}$$

The reason for this phenomenon is differences in spin-orbit coupling, which promotes intersystem crossing. There is strong spin-orbit coupling between two states with different

orbital configurations and weak spin-orbit coupling between two states with the same orbital configuration [15].

Vibronic coupling is a mechanism by which states of the same multiplicity are mixed through vibrations, and the magnitude of vibronic coupling is inversely proportional to the energy separation of the two states [15]. This mechanism can occur between two singlet states or two triplet states. For example, in the case of bdmac, S_1 is (π, π^*) and S_2 is (n, π^*). If the energy gap between these two states is not too large, vibronic coupling can occur, causing S_1 to adopt some (n, π^*) character and S_2 to adopt some (π, π^*) character. Because S_1 now has (n, π^*) character, spin-orbit coupling between S_1 and (π, π^*) triplet states is now more efficient and more likely to occur. As a result, the rate of intersystem crossing increases. This mechanism is known as vibronic spin-orbit coupling [15]. Finally, the energy gap rule states that the efficiency of internal conversion increases as the energy gap between S_0 and S_1 decreases. The reason for this is that there is greater vibrational overlap between S_0 and S_1 as this gap decreases [15].

The scatter plots presented in *Figures 32 – 33* can be divided into two regions. It has been proposed that a different mechanism governs the quantum yields of 2,5-diarylidene cyclopentanones in each region [14]. Vibronic spin-orbit coupling dominates quantum yields in Region 1, which is to the right of the maximum in *Figure 32* and to the left in *Figure 33*. As solvent polarity decreases, S_1 becomes higher in energy and S_2 becomes lower in energy (based on TD-DFT spectral calculations). The S_1 and S_2 states thus become closer in energy, which promotes vibronic spin-orbit coupling. As a result, the rate of intersystem crossing increases, and quantum yields decrease. In terms of increasing solvent polarity, quantum yields increase in this region because the gap between S_1 and S_2 widens, causing vibronic spin-orbit coupling to decrease.

In Region 2, which lies to the left of the maximum in *Figure 32* and to the right in *Figure 33*, the energy gap law dominates quantum yields. S_1 becomes lower in energy with increasing solvent polarity, thereby narrowing the energy gap between S_0 and S_1. According to the energy

gap law, this means that the rate of internal conversion will increase as the gap becomes narrower. As a result, quantum yields decrease with increasing solvent polarity in this region.

Table 10 compares the experimentally-determined photophysical properties of bdmac and Ashrbor. Both compounds show a similar trend in quantum yields; polar protic and nonpolar solvents have low quantum yields, and polar aprotic solvents exhibit the highest quantum yields. Ashrbor has higher quantum yields than bdmac in polar protic and nonpolar solvents but lower quantum yields in polar aprotic solvents. In addition, the quantum yield of Ashrbor in acetonitrile, a polar aprotic solvent, is less than that in isopropanol. Trends in k_{nr} values are similar for both compounds; the greatest values were calculated for ethanol and toluene, while dichloromethane has the lowest value. This trend is inversely related to the trend observed for quantum yields.

Table 10: Experimental photophysical properties of bdmac and Ashrbor

Solvent	**bdmac**				**Ashrbor**			
	Φ_f	τ_f (ns)	k_f (s^{-1})	k_{nr} (s^{-1})	Φ_f	τ_f (ns)	k_f (s^{-1})	k_{nr} (s^{-1})
Methanol	0.036	---	---	---	0.11	---	---	---
Ethanol	0.117	0.46	2.54×10^8	1.92×10^9	0.23	0.82	2.80×10^8	9.39×10^8
Isopropanol	0.2005	---	---	---	0.33	---	---	---
Acetonitrile	0.3395	---	---	---	0.29	---	---	---
Dimethylformamide	0.43	---	---	---	0.36	---	---	---
Dichloromethane	0.4485	1.85	2.42×10^8	2.98×10^8	0.36	1.13	3.19×10^8	5.66×10^8
Ethyl acetate	0.2205	---	---	---	0.2	---	---	---
Toluene	0.076	0.81	9.38×10^7	1.14×10^9	0.11	0.36	3.06×10^8	2.47×10^9
Carbon tetrachloride	0.0345	---	---	---	0.068	---	---	---

*Note 1: Ashrbor data taken from [15]

The values of k_{nr} obtained in a particular solvent for both bdmac and Ashrbor should inversely relate to the quantum yields measured in that solvent and reflect the difference in quantum yield between the two compounds. This was found to be true in two of three instances. Values of k_{nr} reflected quantum yield differences in ethanol and dichloromethane but not in

toluene. The proposed mechanisms governing quantum yields in 2,5-diarylidene cyclopentanones should also explain these differences.

Quantum yields in ethanol are governed by the energy gap rule. Ashrbor has a higher quantum yield than bdmac in this solvent, so the S_1 transition for bdmac should be lower in energy (longer wavelength) than that for Ashrbor. Experimental results do not support this explanation; absorbance maxima for bdmac and Ashrbor in ethanol are 480 nm and 498 nm, respectively. However, this explanation is supported by quantum chemical calculations. The maxima were calculated to be 523 nm (bdmac) and 509 nm (Ashrbor). Values of k_{nr} obtained for the two compounds in ethanol also support the difference in quantum yield. In this case, Ashrbor's k_{nr} value is less than that calculated for bdmac, which increases the quantum yield in comparison to bdmac.

In dichloromethane, bdmac has a higher quantum yield than Ashrbor. Dichloromethane, a polar aprotic solvent, lies in between Regions 1 and 2 for both compounds. Thus either mechanism, or both, could govern the quantum yields. If the energy gap rule dominates, bdmac's S_1 state should be higher in energy (shorter wavelength); this is observed experimentally but not computationally. Experimentally, it was determined that the absorbance maxima for bdmac and Ashrbor in dichloromethane were 470 nm and 484 nm, respectively. However, quantum chemical calculations stated that the maxima are 520 nm (bdmac) and 507 nm (Ashrbor).

If vibronic spin-orbit coupling dominates, it is expected that the $(\pi, \pi^*) \rightarrow (n, \pi^*)$ energy gaps for bdmac are larger than those for Ashrbor, which is true based on computations. For the singlet multiplicity, the energy gaps are 5711 cm^{-1} (bdmac) and 5233 cm^{-1} (Ashrbor); the triplet state energy gaps are 10106 cm^{-1} for bdmac and 9350 cm^{-1} for Ashrbor. The value of k_{nr} calculated for bdmac is also lower than that in Ashrbor, which reflects this difference in quantum yield.

In toluene, however, the calculated k_{nr} values did not reflect differences in quantum yields. Although the quantum yield of Ashrbor in toluene is higher than that of bdmac, the non-radiative rate of decay is greater for Ashrbor. This probably resulted from the unusually long lifetime measured for bdmac in toluene (0.81 ns). It will be necessary in the future to measure this lifetime a second time to ensure that it is reproducible.

Toluene, a nonpolar solvent, is located in Region 1, where vibronic spin-orbit coupling dominates quantum yields. Therefore, it is expected that the (π, π^*) → (n, π^*) energy gaps for bdmac in toluene are lower than those for Ashrbor because Ashrbor's quantum yield is greater. Recall that lower energy gaps promote more vibronic spin-orbit coupling, higher non-radiative rates of decay, and lower quantum yields. For both singlet and triplet multiplicities, TD-DFT spectral calculations show that bdmac's energy gaps (4459 cm^{-1} and 8851 cm^{-1}) are larger than those for Ashrbor (3052 cm^{-1} and 8409 cm^{-1}). It is possible that these energy gaps differ experimentally; however, that cannot be proven because triplet states and forbidden (n, π^*) transitions cannot be observed experimentally.

V. Flash Photolysis and Photochemistry of bdmac

Although a triplet decay curve was generated for TPP in toluene, similar curves could not be generated for bdmac in ethanol or toluene, which must have been due to an extremely short triplet lifetime. This explanation makes sense for the ethanol sample. If the energy gap law governs quantum yields for alcohols, the rate of internal conversion should be relatively high for bdmac in ethanol because the S_1 transition occurs at a low energy. Since vibronic coupling is likely not occurring between the widely-spaced S_1 and S_2 states, the rate of intersystem crossing must be relatively low. Therefore, bdmac should have a very low triplet yield in ethanol. On the other hand, vibronic spin-orbit coupling governs quantum yields in toluene because S_1 and S_2 are close in energy. Therefore, bdmac should have a discernible triplet yield in toluene, and it

would seem reasonable to expect to generate a triplet decay curve using flash photolysis. The fact that no such curve could be obtained may be the result of photochemical processes.

Figure 34 and *Table 11* show the absorbance results from the photochemistry studies conducted for bdmac in toluene. As the irradiation time increases, the optical density of both absorbance bands decreases. This is indicative of a photochemical process, but further experiments are needed to determine exactly what this process is. Because both bands decrease in intensity with increasing irradiation time, photodecomposition may have occurred. In other words, bdmac may have decomposed into other products as it was irradiated.

Photoisomerization is a possibility as well; bdmac has eight photoisomers. The observation that the S_3 band decreases to a lesser extent than the S_1 band supports this hypothesis. As more and more bdmac molecules photoisomerize, there should be a corresponding increase in optical density at the wavelength corresponding to S_1 for the photoisomer, which may be the same wavelength as the S_3 transition of bdmac. If this is the case, the S_3 band of bdmac will be decreasing as the S_1 band of the photoisomer is increasing.

Table 11: Optical density of absorbance bands of bdmac in toluene at various irradiation intervals

Time (min)	**Optical Density**	
	S_1 (λ = 462 nm)	S_3 (λ = 334 nm)
0	0.641627	0.452672
15	0.589770	0.425705
30	0.565301	0.416436
45	0.503250	0.402874
60	0.455534	0.392720

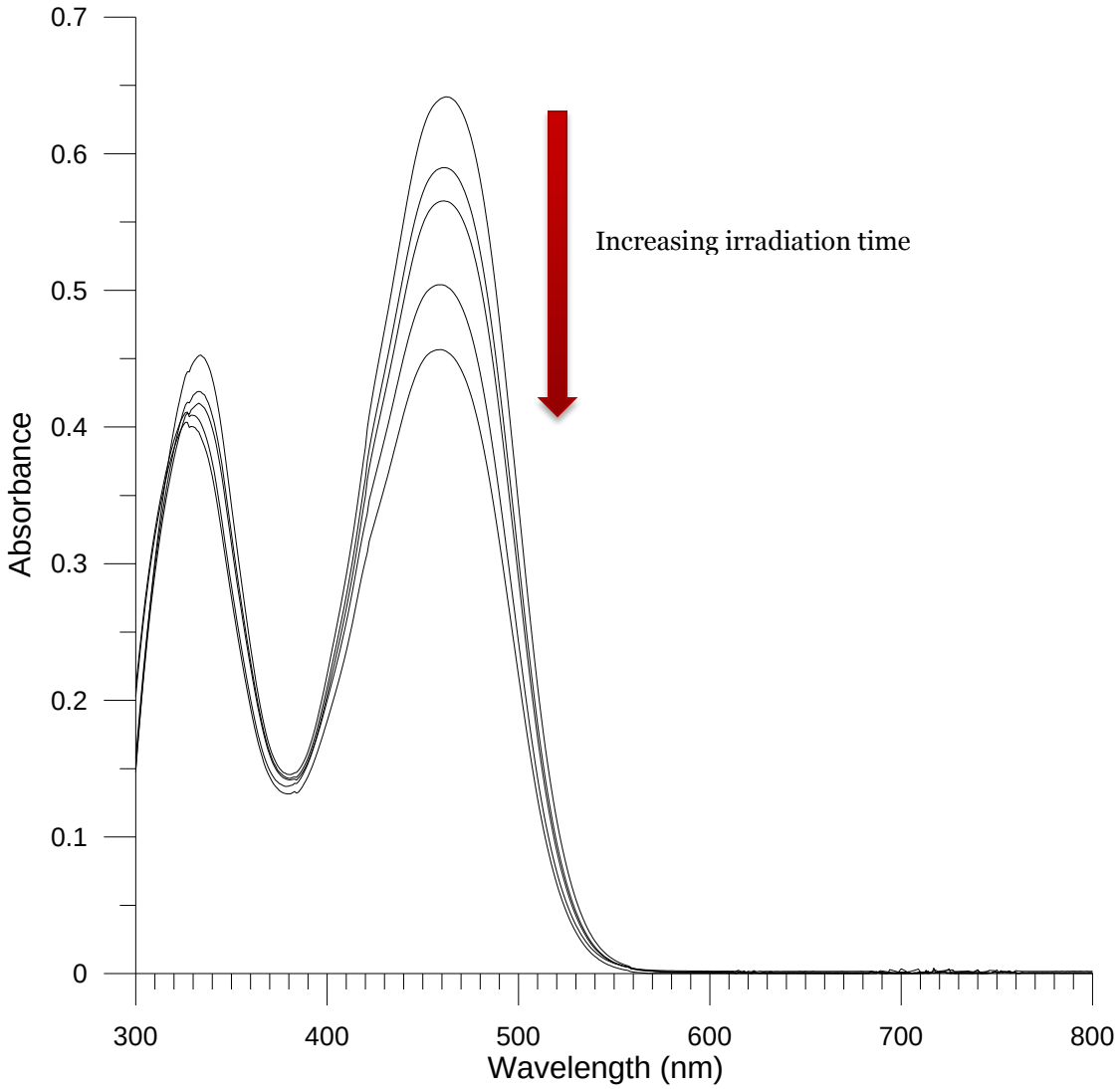

Figure 34: Absorbance spectra of bdmac in toluene under nitrogen at t = 0, 15, 30, 45, and 60 minutes of irradiation

Figure 35 displays the fluorescence emission spectrum of the toluene sample after 60 minutes of irradiation. The spectrum of a non-irradiated sample is also shown for comparison. The emission band appears to be broader in the spectrum of the irradiated sample, which may be a result of photoisomerization. Photoisomers of bdmac may have similar fluorescence maxima, causing the observed band to appear broader. Both samples have the same fluorescence maximum of 550 nm, which supports the hypothesis that bdmac undergoes

photodecomposition under irradiation. More data is needed to determine the processes that are actually occurring.

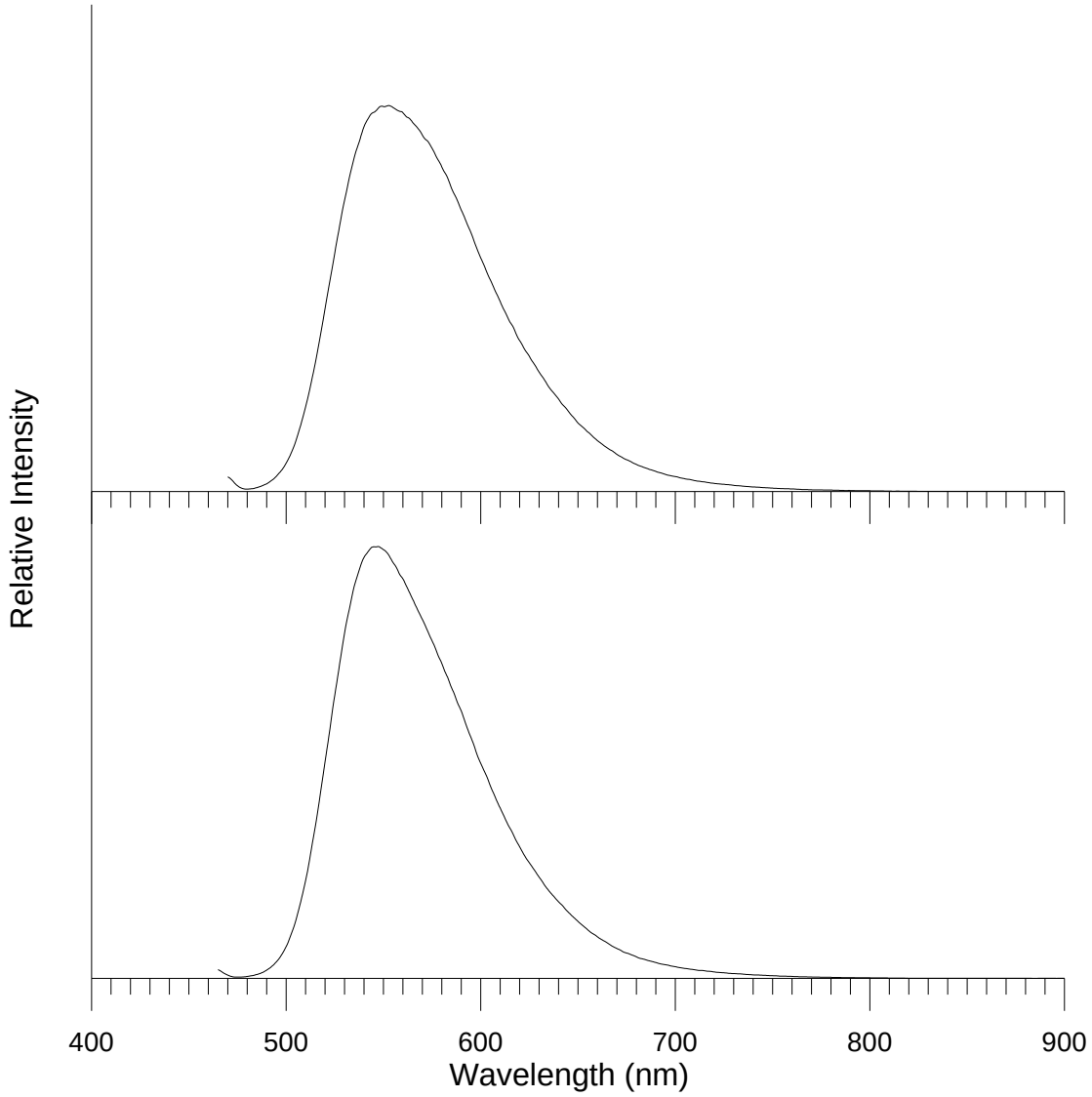

Figure 35: Fluorescence spectra of an irradiated sample (top) and non-irradiated sample (bottom) of bdmac in toluene

Conclusions

Experimental results show that bdmac exhibits solvatochromism. Bathochromic shifts in both absorbance and fluorescence spectral maxima were observed with increasing solvent polarity. A similar trend was observed for Ashrbor, which exhibits lower-energy absorbance maxima than bdmac. However, bdmac fluorescence maxima are more red-shifted than Ashrbor fluorescence maxima, resulting in larger Stokes' shifts for bdmac. Stokes' shifts for both compounds were found to increase as a function of increasing solvent polarity. Bdmac spectral maxima show a linear dependence on the empirical $E_T(30)$ polarity scale, and values of $\Delta\nu$ are linearly dependent on the solvent polarity function.

Fluorescence quantum yields and lifetimes of bdmac also vary with solvent polarity. The roughly bell-shaped relationship between bdmac quantum yields and solvent polarity is consistent with previous postulations that two different mechanisms govern quantum yields in 2,5-diarylidene cyclopentanones. Vibronic spin-orbit coupling appears to dominate in nonpolar solvents, while the energy gap law is likely to dominate in polar protic solvents. Ashrbor shows a similar trend in quantum yields, but it has higher quantum yields than bdmac in alcohols and nonpolar solvents and lower quantum yields in polar aprotic solvents. Values of k_{nr} are inversely related to quantum yields.

Quantum chemical calculations show that bdmac, like Ashrbor, is a charge transfer molecule. Solvent calculations show an increase in μ_g with increasing solvent polarity, which indicates that bdmac interacts more strongly with polar solvents than nonpolar solvents and explains the observed bathochromic shift in spectral maxima. Bdmac has larger ground state dipole moments than Ashrbor, but Ashrbor exhibits a larger change in dipole moment upon excitation and a stronger excited state dipole moment in aprotic solvents.

Because time constraints prevented some experiments from being performed, it is recommended that more data about bdmac be gathered. Additional TD-DFT solvent calculations

should be performed, and fluorescence lifetimes should be measured in more solvents. This will help to further elucidate the relationship between solvent polarity and lifetimes of bdmac. Higher-order partial charge calculations should also be performed, and the use of Ashrbor as a pH probe should be investigated. Further photochemistry studies should be conducted as well. Finally, absorbance and fluorescence spectra of bdmac in methylcyclohexane should be obtained at 77 K in order to determine whether the compound exhibits phosphorescence.

References

[1] Barltrop, J. A., & Coyle, J. D. (1978). *Principles of Photochemistry*. New York: John Wiley & Sons, Inc.

[2] Blais, Z. E. (2012). *Construction of a Flash Photolysis System for Excited State Analysis*. Major Qualifying Project. Worcester Polytechnic Institute.

[3] Chen, Z. (2010). *Synthesis and Properties of a Visible-to-Near-IR-Fluorescing 2,5-Diarylidene Cyclopentanone Charge-Transfer Dye*. Major Qualifying Project. Worcester Polytechnic Institute.

[4] Connors, R. E., & Ucak-Astarlioglu, M. G. (2003). Electronic absorbance and fluorescence properties of 2,5-diarylidene cyclopentanones. *Journal of Physical Chemistry A, 107*, 7684-7691.

[5] Connors, R. E., & Ucak-Astarlioglu, M. G. (2005). Absorbance and fluorescence of 2,5-diarylidenecyclopentanones in acidic media: Evidence for excited state proton transfer. *Journal of Physical Chemistry A, 109*, 8275-8279.

[6] Ewalt, J. R. (2009). *The Synthesis and Spectral Properties of Conjugated Dye Systems*. Major Qualifying Project. Worcester Polytechnic Institute.

[7] Gottlieb, H. E., Kotlyar, V., & Nudelman, A. (1997). NMR chemical shifts of common laboratory solvents as trace impurities. *Journal of Organic Chemistry, 62*, 7512-7515.

[8] Kreher, U. P., Rosamilia, A. E., Raston, C. L., Scott, J. L., & Strauss, C. R. (2003). Direct preparation of monoarylidene derivatives of aldehydes and enolizable ketones with DIMCARB. *Organic Letters, 5*(17), 3107-3110.

[9] Kuhns, M. A. (2010). *Synthesis, Spectroscopic, and Photophysical Properties of an Asymmetrically Substituted 2,5-Diarylidene Cyclopentanone Dye: (2E,5E)-2-(benzofuran-2-ylmethylene)-5-((E)-3-(4-(dimethylamino) phenyl)allylidene)cyclopentanone*. Major Qualifying Project. Worcester Polytechnic Institute.

[10] Lopez, K. (2011). *The Photophysical Properties of a Symmetrically Substituted 2,5 – Diarylidene Cyclopentanone Dye: (2E,5E)-2,5-bis(4-methoxycinnamylidene)-cyclopentanone*. Major Qualifying Project. Worcester Polytechnic Institute.

[11] Roache, M. A. (2010). *Synthesis and Photophysical Properties of an Asymmetrically Substituted 2,5-Diarylidene Cyclopentanone Dye: (2E, 5E)-2-(benzofuran-2-ylmethylene)-5-(4-(dimethylamino)benzylidene)cyclopentanone*. Major Qualifying Project. Worcester Polytechnic Institute.

[12] Silbey, R. J., & Alberty, R. A. (2001). In Harris D., Swain E. and Rigby S. (Eds.), *Physical chemistry* (3rd ed.). New York: John Wiley & Sons, Inc.

[13] Suppan, P., & Ghonheim, N. (1997). *Solvatochromism,* Royal Society of Chemistry, Cambridge, United Kingdom.

[14] Zoto, C. A., & Connors, R. E. (2010). Photophysical properties of an asymmetrical 2, 5-diarylidene-cyclopentanone dye possessing electron donor and acceptor substituents. *Journal of Molecular Structure, 982*(1-3), 121-126. doi: 10.1016/j.molstruc.2010.08.016

[15] Zoto, C. A. (2012). *Structural and Photophysical Properties of Internal Charge Transfer 2-Arylidene and 2,5-Diarylidene Cyclopentanones*, Ph.D. Dissertation, Worcester Polytechnic Institute, 2012.

Appendices

Appendix A: Fluorescence Quantum Yield Sample Calculation

Connors

Quantum yield determination for bdmac in undegassed Dichloromethane with red sensitive tube. Experiment 1

This QuickSheet demonstrates Mathcad's **cspline** and **interp** functions for connecting X-Y data.

Enter a matrix of X-Y data to be interpolated:

Enter spectral data for compound after converting to wavenumbers, multiplying intensity by lambda squared DO NOT normalize intensity. Insert data from Excel -right key, paste table.

data1 :=

1052.63	39200
1030.49	39400
21008.4	39600
0986.36	…

Click on the **Input Table** above until you see the handles, and enlarge it to see the matrix **data** used in this example.

$data1 := csort(data1, 0)$

$X := data1^{\langle 0 \rangle}$ $Y := data1^{\langle 1 \rangle}$

Spline coefficients:

$S1 := cspline(X, Y)$

Fitting function:

$fit(x) := interp(S1, X, Y, x)$

Sample interpolated values:

$fit(21000) = 3.968 \times 10^{4}$

$fit(18800) = 1.709 \times 10^{5}$

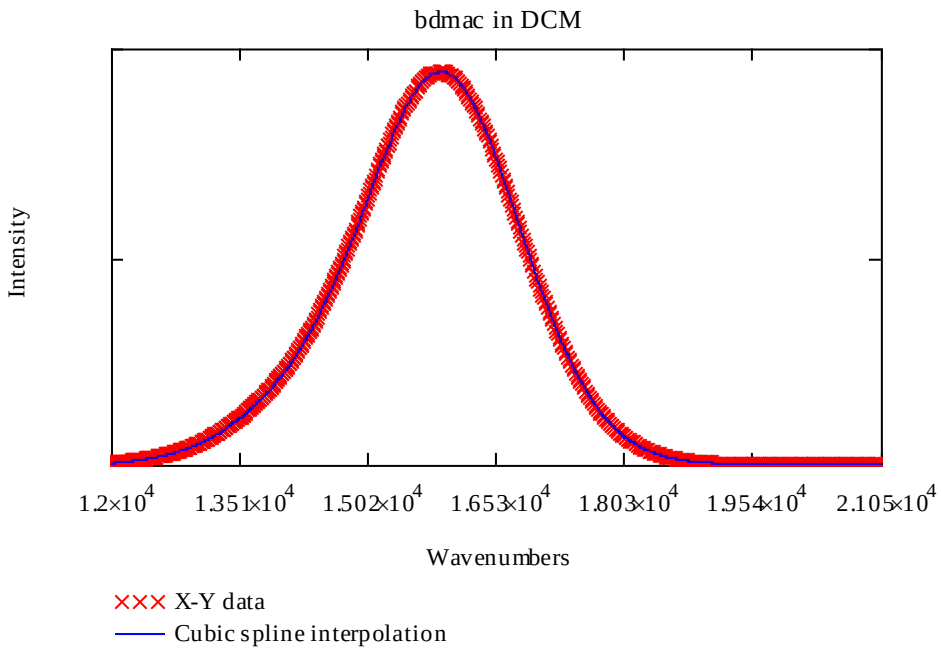

Correction factors for LS50B with red sensitive tube

DATA Limits 12,500-22,200 Wavenumbers

corrdata :=

	0	1
0	12500	19.04
1	12550	…

xdata := csort(corrdata, 0)

A := corrdata⟨0⟩ B := corrdata⟨1⟩

Spline coefficients:

S := cspline(A, B)

Fitting function:

Fitting function:

corrfit(x) := interp(S, A, B, x)

corrspec(x) := corrfit(x)·fit(x)

$l := 12500, 12550 .. 22200$

$l =$

$1.25 \cdot 10^4$
$1.255 \cdot 10^4$
$1.26 \cdot 10^4$
…

$corrspec\ (l) =$

$5.93 \cdot 10^6$
$6.931 \cdot 10^6$
$7.723 \cdot 10^6$
$9.527 \cdot 10^6$
…

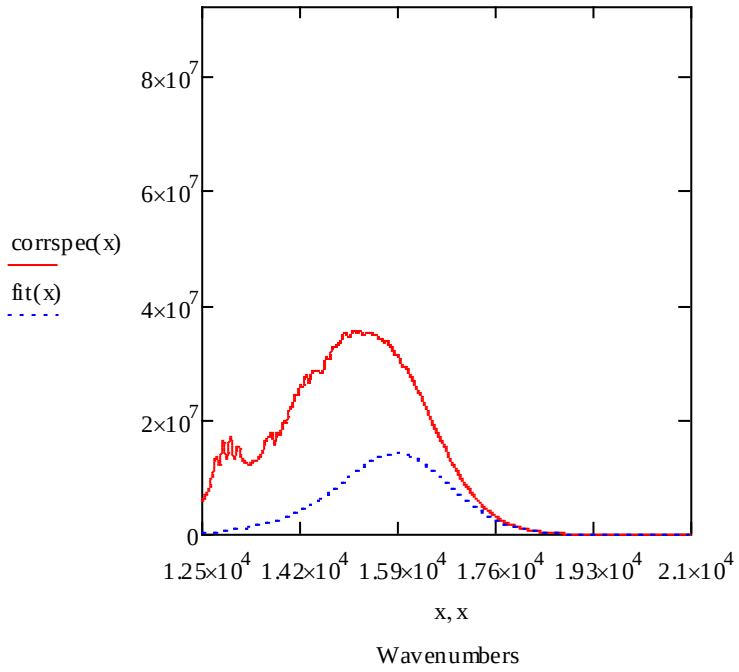

$$\int_{12500}^{21000} fit(x)\,dx = 3.572 \times 10^{10} \qquad \int_{12500}^{21000} corrspec\ (x)\,dx = 1.086 \times 10^{11}$$

Enter a matrix of X-Y data to be interpolated:

Enter spectral data for standard (fluorescein) after converting to wavenumbers, multiplying intensity by lambda squared DO NOT normalize intensities. Insert data from Excel -right key, paste table.

$stdata :=$

21052.63	$1.4 \cdot 10^6$
21030.49	$1.5 \cdot 10^6$
21008.4	…

Click on the **Input Table** above until you see the handles, and enlarge it to see the matrix **data** used in this example.

stdata := csort(stdata, 0)

C := stdata⟨0⟩ D := stdata⟨1⟩

Spline coefficients:

S := cspline(C, D)

Fitting function:

sfit(x) := interp(S, C, D, x)

sfit(18000) = 2.089× 10^7

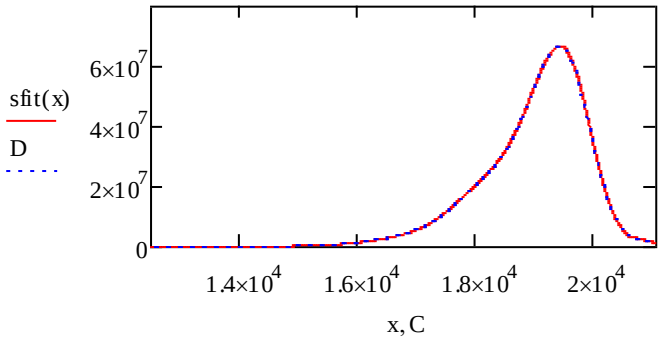

scorrspec(x) := corrfit(x)·(sfit(x))

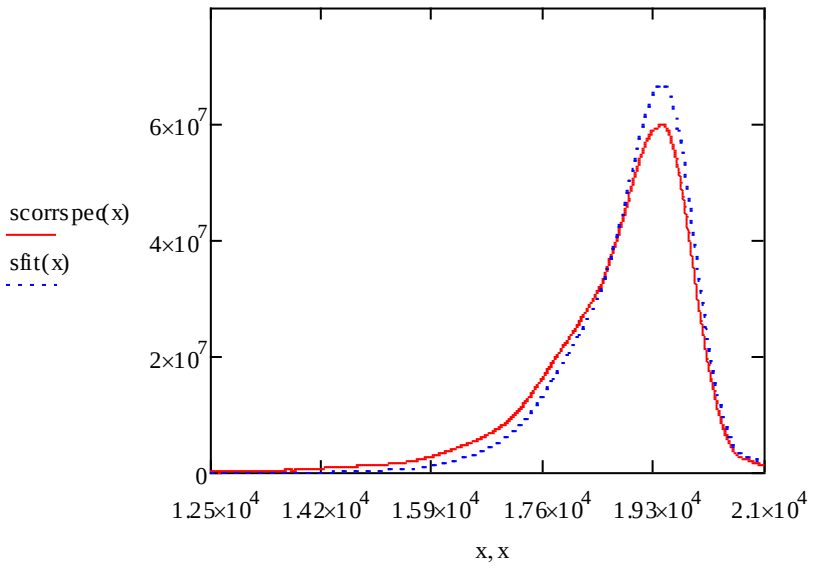

Compound

$$\int_{12500}^{21000} \text{corrspec}(x)\,dx = 1.086\times 10^{11}$$

Standard

$$\int_{12500}^{21000} \text{scorrspec}(x)\,dx = 1.188\times 10^{11}$$

Area under corrected compound curve

$$Dc := \int_{12500}^{21000} \text{corrspec}(x)\,dx$$

$$Dc = 1.086\times 10^{11}$$

Area under corrected standard curve

$$Ds := \int_{12500}^{21000} \text{scorrspec}(x)\,dx$$

$$Ds = 1.188\times 10^{11}$$

	Compound	Standard
Absorbance at (ex)	Ac := 0.051839	As := 0.023923
	DCM	NaOH
Index of refraction	nc := 1.42	ns := 1.33
quantum yield of standard		QYs := 0.9

$$QYc := QYs\cdot\left(\frac{As}{Ac}\right)\cdot\left(nc\cdot\frac{nc}{ns\cdot ns}\right)\cdot\left(\frac{Dc}{Ds}\right)$$

$$QYc = 0.457$$

Appendix B: Fluorescence Lifetime Sample Calculation

Analysis Function : Wed Mar 27 2013 at 15:53

****** one-to-four exponentials ******

***** Input Values *****

Decay curve : A1 470:655_5avg
IRF curve : A1 470:470

Start Time : 37
End Time : 60

Offset will be calculated
Shift will be calculated

Pre-exp. 1 : 1
Lifetime 1 : 1

***** Statistics *****

Job done after 6 iterations in 0.047 sec.

Fitted curve : FLD Fit (7)
Residuals : FLD Residuals (7)
Autocorrelation : FLD Autocorrelation (7)
Deconvolved Fit : FLD Deconvoluted (7)

Chi2 : 3.877
Durbin Watson : 0.5979
Z : -0.3406

Pre-exp. 1 : 1.169 ± 6.221e-003 (100 ± 0.5323%)
Lifetime 1 : 1.842 ± 6.948e-003

F1 : 1
Tau-av1 : 1.842
Tau-av2 : 1.842
Offset : -6.03
Shift : 0.4729

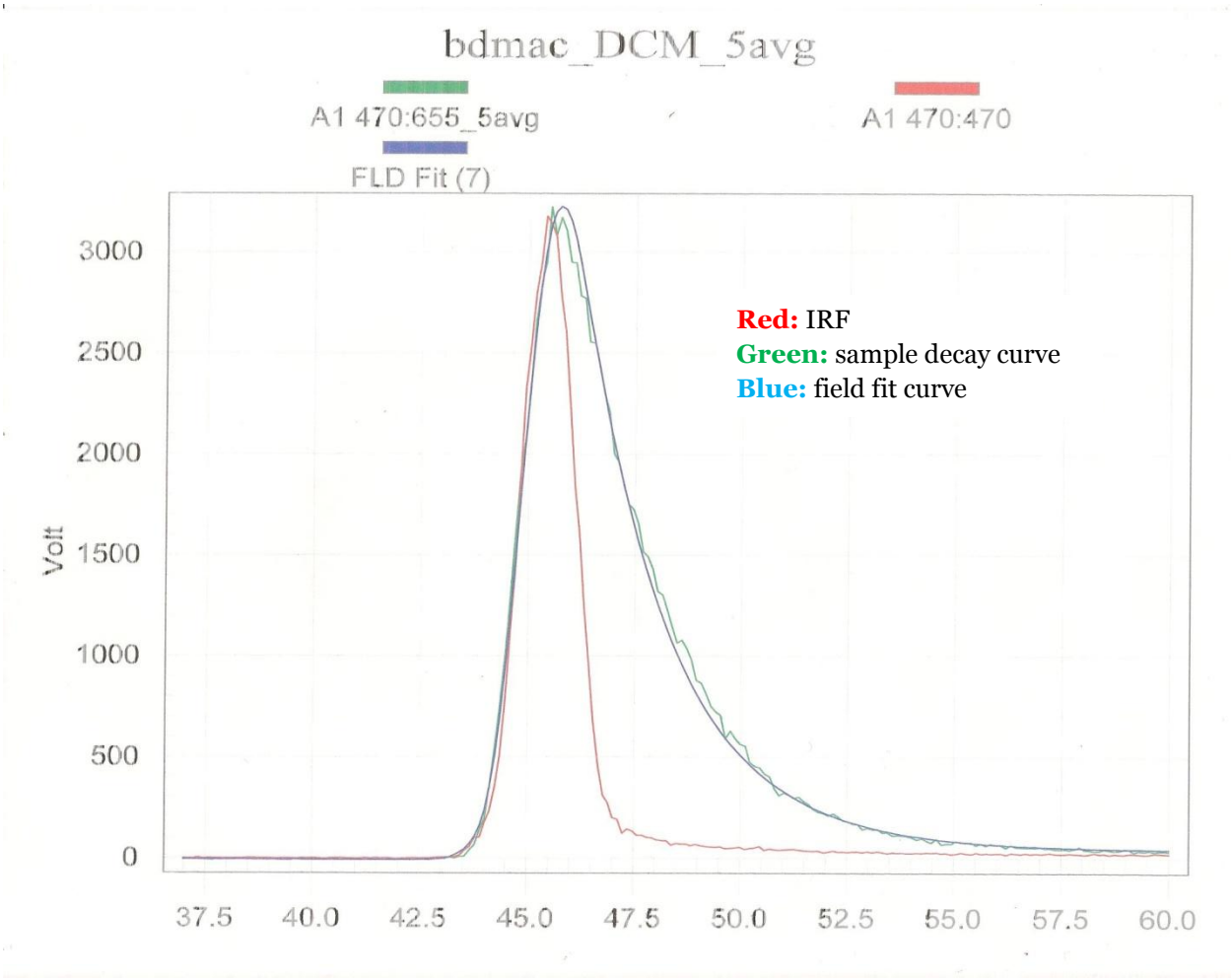

Figure 36: Fluorescence decay profile of bdmac in dichloromethane

Appendix C: Spectroscopic and Photophysical Data

I. bdmac

Table 12: Experimental spectroscopic and photophysical properties of bdmac

Solvent	ν_{abs} (cm^{-1})	ν_f (cm^{-1})	$\Delta\nu$ (cm^{-1})	$E_T(30)$ (kcal/mol)	Δf	Φ_f	τ_f (ns)	k_f (s^{-1})	k_{nr} (s^{-1})
HOAc	20576	14166	6410	---	---	---	---	---	---
MeOH	20790	13996	6794	55.4	0.3093	0.036	---	---	---
EtOH	20833	14187	6646	51.9	0.2887	0.117	0.46	2.54×10^8	1.92×10^9
1-PrOH	20790	14217	6573	50.7	0.2746	---	---	---	---
2-PrOH	20964	14248	6716	48.4	0.2769	0.2005	---	---	---
ACN	21645	14298	7347	45.6	0.3054	0.3395	---	---	---
DMF	21186	14319	6867	43.2	0.2752	0.43	---	---	---
DCM	21276	15254	6022	40.7	0.2171	0.4485	1.85	2.42×10^8	2.98×10^8
EtOAc	22075	16180	5895	38.1	0.1996	0.2205	---	---	---
Toluene	21881	17184	4697	33.9	0.0131	0.076	0.81	9.38×10^7	1.14×10^9
CS_2	21141	17141	4000	32.8	-0.0007	---	---	---	---
CCl_4	22271	17966	4305	32.4	0.0119	0.0345	---	---	---
n-hexane	22988	19272	3716	31	-0.0004	---	---	---	---

II. Ashrbor

Table 13: TD-DFT spectral calculations for Ashrbor

Solvent	Transition	Transition energy			f	CI	MO
		eV	*λ (nm)*	*ν (cm^{-1})*			
Gas (μ_g = 5.60 D)	T_1 (π, π^*)	1.664	745.09	13421	0	0.61125	100-101
	T_2 (π, π^*)	2.0846	594.76	16814	0	0.56714	99-101
	T_3 (n, π^*)	2.5726	481.94	20749	0	0.68522	98-101
	S_1 (π, π^*)	2.7088	457.71	21849	1.7599	0.69588	100-101
	S_2 (n, π^*)	2.9047	426.84	23428	0.0002	0.69472	98-101
	T_4 (π, π^*)	3.0271	409.58	24415	0	0.52421	97-101
	S_3 (π, π^*)	3.073	403.46	24786	0.0544	0.67424	99-101
	T_5 (π, π^*)	3.1642	391.83	25521	0	0.51453	100-102
	S_4 (π, π^*)	3.4511	359.26	27835	0.2355	0.55654	100-102
	S_5 (π, π^*)	3.5716	347.14	28807	0.1518	0.55528	97-101
	T_1 (π, π^*)	1.6451	753.65	13269	0	0.62426	100-101

Toluene (μ_g = 6.57 D)	T_2 (π, π^*)	2.0608	601.64	16621	0	0.58779	99-101
	S_1 (π, π^*)	2.5063	494.68	20215	1.9952	0.70144	100-101
	T_3 (n, π^*)	2.6878	461.29	21678	0	0.68668	98-101
	S_2 (π, π^*)	2.933	422.72	23656	0.0485	0.69253	99-101
	T_4 (π, π^*)	2.9796	416.12	24032	0	0.57902	97-101
	S_3 (n, π^*)	3.0088	412.08	24267	0.0001	0.69484	98-101
	T_5 (π, π^*)	3.0965	400.4	24975	0	0.58227	100-102
	S_4 (π, π^*)	3.4144	363.13	27538	0.0963	0.68227	100-102
	S_5 (π, π^*)	3.5268	351.55	28445	0.2417	0.62277	97-101
Dichloromethane (μ_g = 7.47 D)	T_1 (π, π^*)	1.6212	764.76	13076	0	0.63502	100-101
	T_2 (π, π^*)	2.0322	610.09	16391	0	0.60529	99-101
	S_1 (π, π^*)	2.4445	507.19	19716	1.9906	0.70212	100-101
	T_3 (n, π^*)	2.7805	445.91	22426	0	0.68676	97-101
	S_2 (π, π^*)	2.8735	431.48	23176	0.0468	0.69308	99-101
	T_4 (π, π^*)	2.9212	424.42	23562	0	0.5903	98-101
	T_5 (π, π^*)	3.0497	406.54	24598	0	0.60382	100-102
	S_3 (n, π^*)	3.0934	400.81	24949	0	0.6955	97-101
	S_4 (π, π^*)	3.3795	366.87	27258	0.1529	0.64003	100-102
	S_5 (π, π^*)	3.4902	355.24	28150	0.1907	0.5982	98-101
Ethanol (μ_g = 7.76 D)	T_1 (π, π^*)	1.6126	768.82	13007	0	0.63812	100-101
	T_2 (π, π^*)	2.0221	613.14	16309	0	0.61043	99-101
	S_1 (π, π^*)	2.4343	509.33	19634	1.9763	0.70226	100-101
	T_3 (n, π^*)	2.807	441.7	22640	0	0.68764	97-101
	S_2 (π, π^*)	2.8603	433.47	23070	0.0455	0.69222	99-101
	T_4 (π, π^*)	2.9018	427.27	23404	0	0.59	98-101
	T_5 (π, π^*)	3.0371	408.23	24496	0	0.60459	100-102
	S_3 (n, π^*)	3.1176	397.69	25145	0	0.69637	97-101
	S_4 (π, π^*)	3.3688	368.03	27172	0.2345	0.52693	100-102
	S_5 (π, π^*)	3.4814	356.13	28080	0.1119	0.50615	98-101

*Note 1: Data collected by Christopher Zoto, Ph.D.

Table 14: Experimental spectroscopic and photophysical properties of Ashrbor

Solvent	ν_{abs} (cm^{-1})	ν_f (cm^{-1})	$\Delta\nu$ (cm^{-1})	$E_T(30)$ (kcal/mol)	Δf	Φ_f	τ_f (ns)	k_f (s^{-1})	k_{nr} (s^{-1})
MeOH	20000	13570	6430	55.4	0.3093	0.11	0.30	3.67×10^8	2.97×10^9
EtOH	20080	13790	6290	51.9	0.2887	0.23	0.82	2.80×10^8	9.39×10^8
1-PrOH	20040	13953	6087	50.7	0.2746	0.34	1.13	3.01×10^8	5.84×10^8
2-PrOH	20284	14557	5727	48.4	0.2769	0.33	1.24	2.66×10^8	5.40×10^8
ACN	20921	15016	5905	45.6	0.3054	0.29	0.91	3.19×10^8	7.80×10^8
DMF	20576	15237	5339	43.2	0.2752	0.36	1.32	2.73×10^8	4.85×10^8
DCM	20661	15747	4914	40.7	0.2171	0.36	1.13	3.19×10^8	5.66×10^8
EtOAc	21552	16920	4632	38.1	0.1996	0.2	0.71	2.82×10^8	1.13×10^9
Toluene	21053	18858	2195	33.9	0.0131	0.11	0.36	3.06×10^8	2.47×10^9
CS_2	20450	18518	1932	32.8	-0.0007	0.13	0.43	3.02×10^8	2.02×10^9
CCl_4	22272	19402	2870	32.4	0.0119	0.068	0.29	2.34×10^8	3.21×10^9
n-hexane	22989	19844	3145	31	-0.0004	0.007	---	---	---

*Note 1: Data taken from [15]